1   **Neuroinflammation and EIF2 signaling persist in an HiPSC tri-culture model of HIV infection**

2   **despite antiretroviral treatment**

3

4   Sean K. Ryan[1,2], Michael V. Gonzalez[6], James P. Garifallou[6], Frederick C. Bennett[3], Kimberly S.

5   Williams[5], Hakon Hakonarson[6,7], Stewart A. Anderson[2,3]*, Kelly L. Jordan-Sciutto[1,4]*

6

7   1. Department of Pathology, Perelman School of Medicine, University of Pennsylvania,

8   Philadelphia, PA 19104, USA

9   2. Department of Psychiatry, The Children's Hospital of Philadelphia, Philadelphia, PA

10   19104, USA

11   3. Department of Psychiatry, Perelman School of Medicine, University of Pennsylvania,

12   Philadelphia, PA 19104, USA

13   4. Department of Basic and Translational Sciences, School of Dental Medicine, University

14   of Pennsylvania, Philadelphia, PA 19104, USA

15   5. Environmental and Health Sciences Program, Spelman College, Atlanta, GA 30314, USA

16   6. Center for Applied Genomics, Children's Hospital of Philadelphia, The Perelman School

17   of Medicine, University of Pennsylvania, Philadelphia, PA, USA

18   7. Division of Human Genetics, Department of Pediatrics, The Perelman School of

19   Medicine, University of Pennsylvania, Philadelphia, PA, USA

20   * Stewart A. Anderson and Kelly L. Jordan-Sciutto should be considered joint senior author.

21   **Competing Interests**

22   The authors declare no competing interests.

Abstract

HIV-Associated Neurocognitive Disorders (HAND) affect over half of HIV-infected individuals worldwide, despite antiretroviral therapy (ART). Therapeutically targetable mechanisms underlying HAND remain elusive. We developed a human-induced pluripotent stem cell (HiPSC) based model; whereby, we independently differentiate HiPSCs into neurons, astrocytes, and microglia and systematically combine to generate a tri-culture with or without HIV-infection and ART. scRNAseq analysis on tri-cultures including HIV-infected microglia revealed inflammatory signatures in the microglia and EIF2 signaling in all three cell types. Remarkably, EFZ alone induced a similar response to infection. Treatment with the antiretroviral compound Efavirenz (EFZ) mostly resolved these signatures; However, EFZ increased RhoGDI and CD40 signaling in the HIV-infected microglia. This activation was associated with a persistent increase in TNFa expression. This work establishes a tri-culture that recapitulates key features of HIV infection in the CNS and provides a new model to examine the effects of HIV infection and its treatment with antiretrovirals.

Introduction

HIV-Associated Neurocognitive Disorders (HAND) are a chronic, progressing spectrum of diseases that lead to a range of neurologic disorders, including HIV-associated dementia. The major pathologic manifestation that persists in HAND patients with antiretroviral treatment (ART) is synaptodendritic damage and the accumulation of microglia, the immune cell in the central nervous system (CNS); however, the mechanisms underlying synaptic damage remain elusive. Synapse loss is associated with infiltration of macrophages from outside of the CNS and activation of microglia. Both HIV-infected macrophage populations can release cytokines, viral proteins, and excitotoxins, which can lead to synaptic damage (Saylor et al., 2016). Activated microglia aberrantly phagocytosing synapses have been described in multiple neurological disorders including: Alzheimer's, Frontotemporal Dementia, and Multiple Sclerosis (Keren-Shaul et al., 2017; Lui et al., 2016; Salter & Stevens, 2017; Zrzavy et al., 2017). While patients on ART experience milder forms of HAND, they still experience chronic inflammation (Kolson, 2017). Infected microglia and uninfected, but active microglia may be working in tandem to slowly release proinflammatory cytokines and reactive oxygen species that, over time, can lead to synaptodendritic damage.

Inflammation, via various pathways, plays a large role in the neurodegeneration seen in HAND. Our lab and others have implicated the unfolded protein response (UPR), a part of the integrated stress response (ISR) in neurodegeneration including in HAND (Walter & Ron, 2011). EIF2 activation, downstream of UPR activation, has been implicated in HAND (C. Akay et al., 2012; K. A. Lindl, Akay, Wang, White, & Jordan‐Sciutto, 2007), progressive supranuclear palsy and Alzheimer's disease (Stutzbach et al., 2013). CD40 has also been implicated in viral replication control and microglia activation during HIV infection (D'Aversa, Eugenin, & Berman, 2008; Kornbluth, 2000; Sui et al., 2007). CD40 signaling is implicated in multiple cellular processes including inflammatory response. Specifically, CD40 activation can lead to, CD40 activation can lead to activation of the NF-κB non canonical pathway and the production of IL-8 and TNFa (D'Aversa et al., 2008; Homig-Holzel et al., 2008). TNFa, in turn, can activate the NADPH oxidase complex (Y.-S. Kim, Morgan, Choksi, & Liu, 2007). Similarly, RhoGDI normally anchors Rac1, but during inflammation, Rac1 is released from RhoGDI and moves to the plasma membrane where

3

66   it interacts with the NADPH oxidase complex which creates superoxide when activated

67   (Wilkinson & Landreth, 2006) and regulates cytokine and neurotoxin release by microglia

68   exposed to HIV-Tat (Turchan–Cholewo et al., 2009). Understanding how various endogenous

69   pathways may influence HAND using a therapeutic relevant model is important.

70   While the major pathological manifestation of HAND is synaptodendritic damage, the

71   response during initial exposure to HIV and ART is unknown partly because current models for

72   HIV-mediated neuroinflammation are limited by species differences and human tropism of the

73   virus. For instance, the HIV-1 Tat transgenic mouse model exhibits neuroinflammation and

74   behavioral deficits, but only expresses a single viral protein from astrocytes (Carey, Sypek, Singh,

75   Kaufman, & McLaughlin, 2012; B. O. Kim et al., 2003; Langford et al., 2018). Another HIV-1

76   transgenic mouse model has neuroinflammation, but is missing two of the genes, *gag* and *pol*,

77   and is expressed in every cell in the body (Reid et al., 2001). Lastly, while isolated microglia from

78   human patients can give great insight, it is only a snapshot of the end stage of the disease.

79   Therefore, the development of a novel *in vitro* human system allowing the interaction of the main

80   cell types involved in HAND is needed to further understand the neuropathogenesis and develop

81   novel therapeutics.

82   We have developed a Human-induced pluripotent stem cell (HiPSC) based model whereby

83   we separately differentiate HiPSCs into forebrain-like excitatory neurons, astrocytes, and

84   microglia then combine them to create a tri-culture, with or without HIV-infection of the

85   microglia, and with or without ART. Our protocol rapidly produces microglia-like cells (iMg) that

86   express multiple classical markers in mono-culture, productively infect with HIV, and respond to

87   ART. In addition, we have developed a differentiation protocol for astrocyte-like cells (iAst) that

88   express hallmark proteins. Utilizing this system, we investigated the effects of Infection (Inf),

89   Infection with the antiretroviral Efavirenz (EFZ) (Inf+EFZ), and EFZ treatment alone (Uninf+EFZ),

90   compared to uninfected tri-cultures (Uninf) and to each other. We found that EFZ treatment in

91   infected conditions did not simply attenuate the inflammatory response but created a distinct

92   reaction. In addition, EFZ treatment alone invoked its own discrete inflammatory response. We

93   revealed gene expression changes leading to activation of EIF2 signaling in iMg, iAst, and iNrn,

94   and highly activated inflammatory cytokine signaling in iMg in the Inf condition. EIF2 signaling

95   persisted exclusively in the iNrns in the Inf+EFZ condition. While infection lead to increased

96   inflammation in the iMg, it also led to decreased synaptophagy. EFZ treatment in infected

97   cultures did not reverse the phagocytosis impairment but did quell the inflammation except for

98   distinct gene activation of CD40 and RhoGDI signaling in the iMg. Lastly EFZ treatment itself lead

99   to a very similar response as Inf. Our system has reveals the complex roles of the individual cell

100   types during infection ± ART and how ART alone can elicit an inflammatory response.

Results
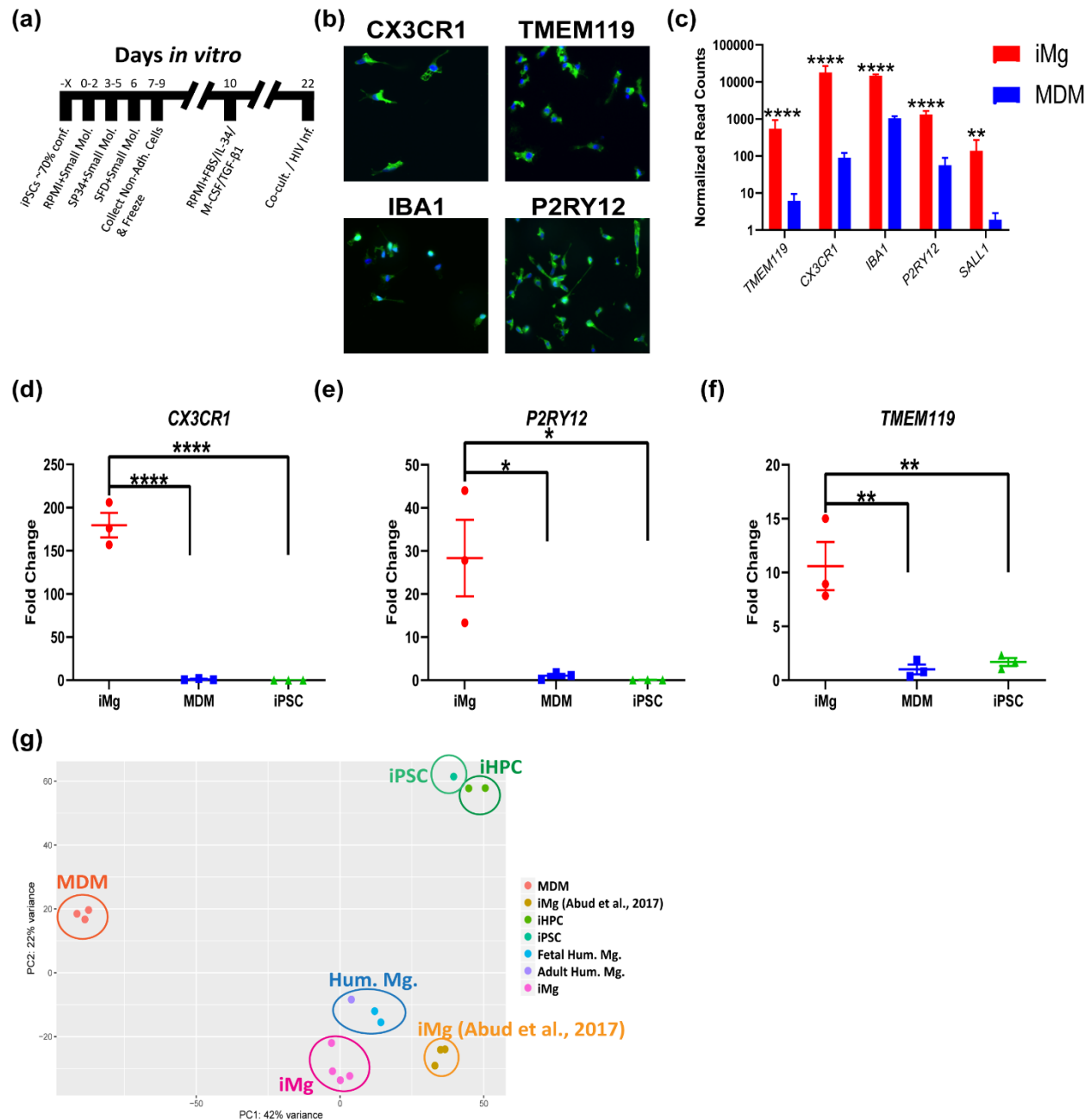
Figure 1: Generation and characterization of iMg

(a) Timeline for iMg differentiation and HIV infection. (b) Immunostaining for microglia specific markers: CX3CR1, TMEM119, IBA1, and P2RY12. All cultures were stained for DAPI. (c) Bulk RNAseq normalized read counts of specific microglia markers from iMg and MDMs. n=4 iMg, n=3 MDMs. Benjamini-Hochberg, FDR 0.01, **p<0.01, ****p<0.0001, error bars represent SEM. (d-f) qRT-PCR validation for expression of *CX3CR1* (d), *P2RY12* (e), and *TMEM119* (f) in iMg. Probes normalized to *GAPDH* expression. n=3 cell lines, one-way ANOVA, Dunnett's post hoc analysis, *p<0.05; **p<0.01, ****p<0.0001, error bars represent SEM. (g) PCA for monocyte-derived macrophages, iMicroglia, and (Abud et al., 2017) iMg, iPSC, iHPC, and primary human microglia. Each dot represents a bulk RNAseq sample. MDM - monocyte-derived macrophage; iHPC – induced hematopoietic progenitor cells. iPSC, iHPC, Hum. Mg., iMg (Abud et al., 2017) samples were all retrieved from (Abud et al., 2017).

6

114 **iMicroglia exhibit similar gene and protein expression as other iPSC-derived microglia**

115   We modified two previously published protocols to generate the iMg (Abud et al., 2017;

116 Paluru et al., 2014) (Figure 1a). The first step is a nine-day differentiation of iPSCs into

117 CD41+CD235+ common myeloid progenitors (CMPs) (Paluru et al., 2014). The second step is a

118 modified 11-day protocol (Abud et al., 2017) that produces a highly pure population of iMg. We

119 tested this protocol on four separate cell lines. These iMg show ramification (Figure 1-figure

120 supplement 1a), express several classical markers, including: CX3CR1, IBA1, and P2RY12, at the

121 protein and RNA level (Figures 1b and 1c) in mono-culture, and have a significantly different gene

122 expression profile than monocyte-derived macrophages (MDMs) (Figure 1-figure supplement

123 1b). We validated the findings in BulkRNAseq with qRT-PCR. The iMg exhibited a 179-fold, 28-

124 fold, and 11-fold increase in *CX3CR1*, *P2RY12*, and *TMEM119* respectively over MDMs (Figure 1d-

125 1f). Importantly they also express CCR5 (Figure 1-figure supplement 1c), one of the co-receptors

126 necessary for HIV infection (Deng et al., 1996). Utilizing PCA, we compared our iMg to human

127 MDMs we generated and the primary human adult and fetal microglia, iPSCs, induced

128 hematopoietic progenitor cells, and iMicroglia from (Abud et al., 2017). PCA revealed considerate

129 clustering of our iMg (pink) to the primary human microglia (blue) and previously published iPSC-

130 derived microglia (light orange) (Figure 1g).
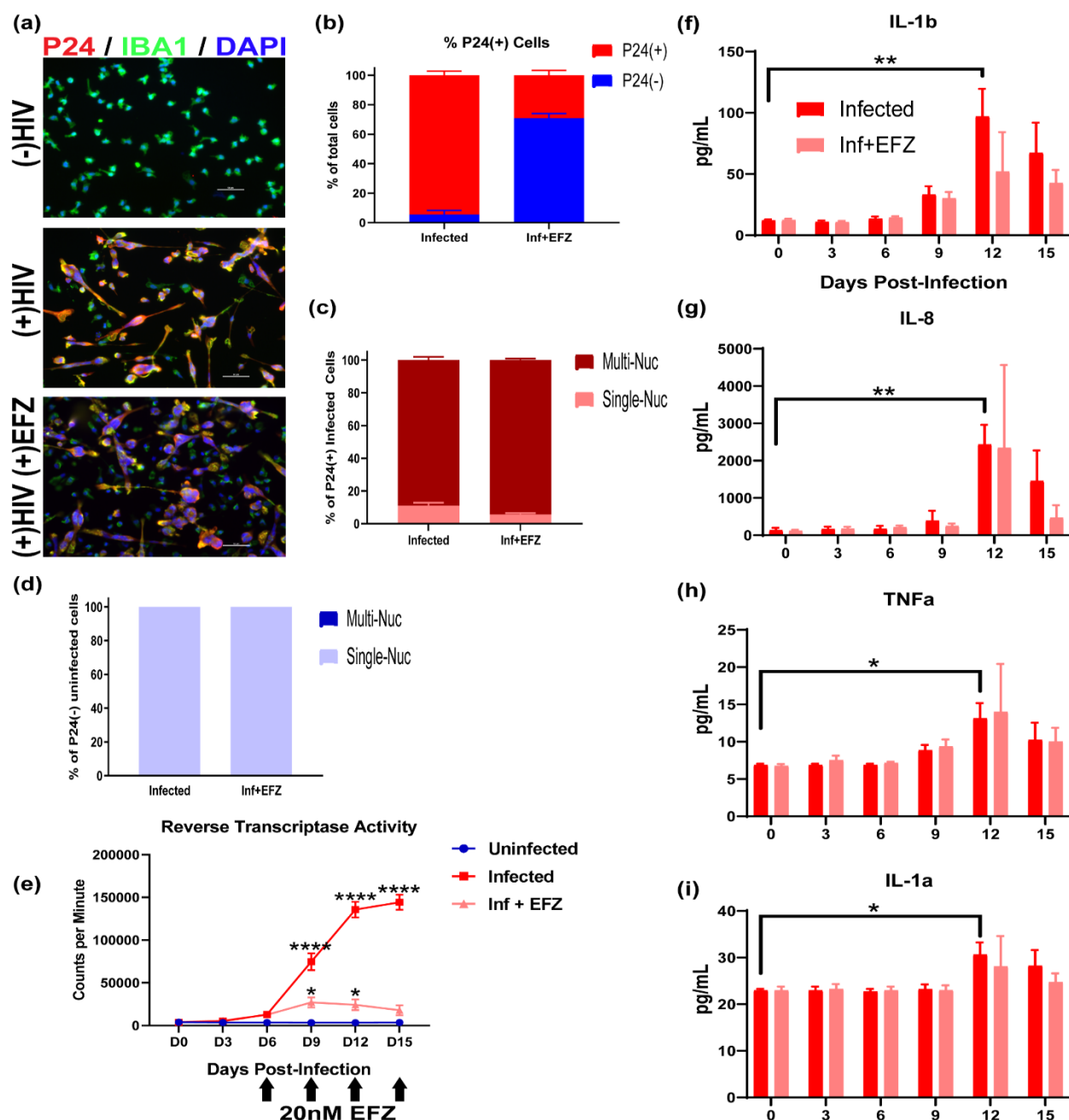
Figure 2: iMicroglia are infected by HIV, produce an inflammatory response, and respond to EFZ

(a) Immunostaining showing reduced percentage of P24+(red) IBA1+(green) iMg in HIV-infected mono-cultures + EFZ treatment compared to infected cultures with no EFZ treatment. (b) Percentage of P24+ cells in mono-culture iMg at D15 for infected and Inf+EFZ conditions. n=4 infections, error bars represent SEM. (c) Percent of P24+ single-nucleated and multi-nucleated iMg in mono-culture for infected and Inf+EFZ conditions. n=4 infections. (d) Percent of P24(-) single-nucleated and multi-nucleated iMg in mono-culture for Inf and Inf+EFZ conditions. n=4 infections. (e) Reverse transcriptase activity of Uninf, Inf, and Inf+EFZ (20nM) iMg show productive infection and response to EFZ. n=3 infections, one-way ANOVA, Dunnett's post hoc analysis, *p<0.05; ****p<0.0001, error bars represent SEM. (f-i) Cytokine analysis of Infected iMg mono-culture displays increase in IL-1b (f), IL-8 (g), TNFa (h), and IL-1a (i) production in the infected iMg. n=4 infections, one-way ANOVA, Dunnett's post hoc analysis, *p<0.05; **p<0.01, error bars represent SEM.

8

144   **iMg Are productively infected with HIV and respond to multiple antiretrovirals**

145   We investigated the effects of HIV infection and ART in an iMg mono-culture. We first

146   determined infectivity of the iMg. We exposed the iMg to 50ng/mL of the CSF-derived, R5-tropic

147   JAGO strain of HIV (Chen et al., 2002). We performed a 15-day infection, based on prior studies

148   of MDMs (O'Donnell et al., 2006) which resulted in 94.5 ± 5.5% of the iMg positive for the HIV

149   capsid protein P24 (Figures 2a and 2b) and exhibited vast syncytia (Figure 2-figure supplement

150   1b). 89.1 ± 3.8% of P24(+) iMg were multi-nucleated (Figure 2c), and 100% of P24(-) iMg were

151   single-nucleated (Figure 2d). Reverse transcriptase activity showed peak viral production

152   occurred near day 15 (Figure 2e). iPSCs did not become infected at this concentration (Figure 2-

153   figure supplement 2b). We infected four separate iMg lines; however, one was heterozygous for

154   the CCR5Δ32 mutation, leading to impaired infection (Liu et al., 1996) (Figure 2-figure

155   supplement 2c and 2d). Therefore, we excluded it from all future analysis. To our knowledge, this

156   this the first time iPSC-derived microglia have been infected with HIV.

157   We tested two antiretroviral treatments that target different parts of the HIV life cycle,

158   Darunavir (DRN) and efavirenz (EFZ) (Figure 2-figure supplement 2a). DRN is a protease inhibitor

159   that prevents assembly of new virus (Wood & Flexner, 1998), and EFZ is a non-nucleoside reverse

160   transcriptase inhibitor that prevents reverse transcription of the viral genome (De Clercq, 2004).

161   We opted to focus on EFZ, as it is still a first line drug in many parts of the world (Best &

162   Goicoechea, 2008; Taramasso et al., 2018), Further, because it blocks HIV infection at the reverse

163   transcription phase, we can study non-productively infected, HIV-exposed cells alongside

164   productively infected cells.. Importantly, the infected iMg responded as expected to EFZ (Figures

165   2a, 2b, and Figure 2-figure supplement 2a). At day 15, 29.2 ± 6.3% of the iMg were infected

166   (Figures 2d and Figure 2-figure supplement 1c). 94.4 ± 1.72% of P24(+) iMg in the infected + EFZ

167   mono-culture were multi-nucleated (Figure 2d), and 100% of P24(-) iMg in the infected + EFZ

168   mono-culture were single-nucleated, same as the infected condition (Figure 2e).

169

170   **Infected iMg produced proinflammatory cytokines at peak infection, and EFZ treatment**

171   **reduced the response**

172   We also explored the changes in cytokine production over the course of infection ± EFZ.

173   Infection led to increased production of several pro-inflammatory cytokines, specifically IL-1b, IL-

174   1a, TNFa, and most prominently, IL-8 (Figures 2f-2i). However, the two other cytokines tested: IL-

175   6 and IL-10, did not change across any condition (Figure 2-figure supplement 3a-3c). IL-8

176   production was increased in cultured, infected, fetal microglia (Tatro, Soontornniyomkij,

177   Letendre, & Achim, 2014), and IL-1b RNA was increased in laser-captured microglia from brain

178   samples of HIV-infected patients (Ginsberg et al., 2018). Infected iMg cultures exposed to EFZ

179   had mitigated, non-significant responses to IL-1b, IL-8, TNFa, and IL-1a (Figures 2f-2i), suggesting

180   a reduced inflammatory reaction. Uninf, Uninf+EFZ and the DMSO vehicle control did not

181   elucidate a cytokine reaction across the six cytokines tested (Figure 2-figure supplement 3a-3e

182   and Figure 2-figure supplement 4a-4d).

183

184   **Infected iMg have impaired cell cycle regulation and DNA repair and increased expression of**

185   **inflammatory genes**

186   Bulk RNAseq of three iMg lines ± HIV infection revealed significant changes in cell cycle

187   regulation and DNA repair (Figure 2-figure supplement 5a). Infected immune cells will die quickly

188   after infection (Cummins & Badley, 2010), and we observed a high percentage of giant multi-

189   nucleated cells. Thus, it is unsurprising to see that most of the top canonical pathways altered

190   involved cell cycle and DNA repair. While no inflammatory pathways were identified by IPA

191   analysis, many inflammatory genes involved in the complement system, NF-κB signaling, and

192   TNFa signaling were significantly upregulated (Figure 2-figure supplement 5c). In addition, other

193   inflammatory genes including *IL1b*, *CCL8*, and *FOS* were also upregulated (Figure 2-figure

194   supplement 5c).

195   Collectively, these data show that the iMg exhibit an inflammatory response similar to the

196   that seen in the brain with increased production of IL-8, IL-1b, IL-1a, and TNFa. This inflammatory

197   response is strongly attenuated with Efavirenz treatment. Bulk RNAseq analysis revealed changes

198   in cell cycle and inflammation between uninfected and infected iMg, as expected.

199

10

200
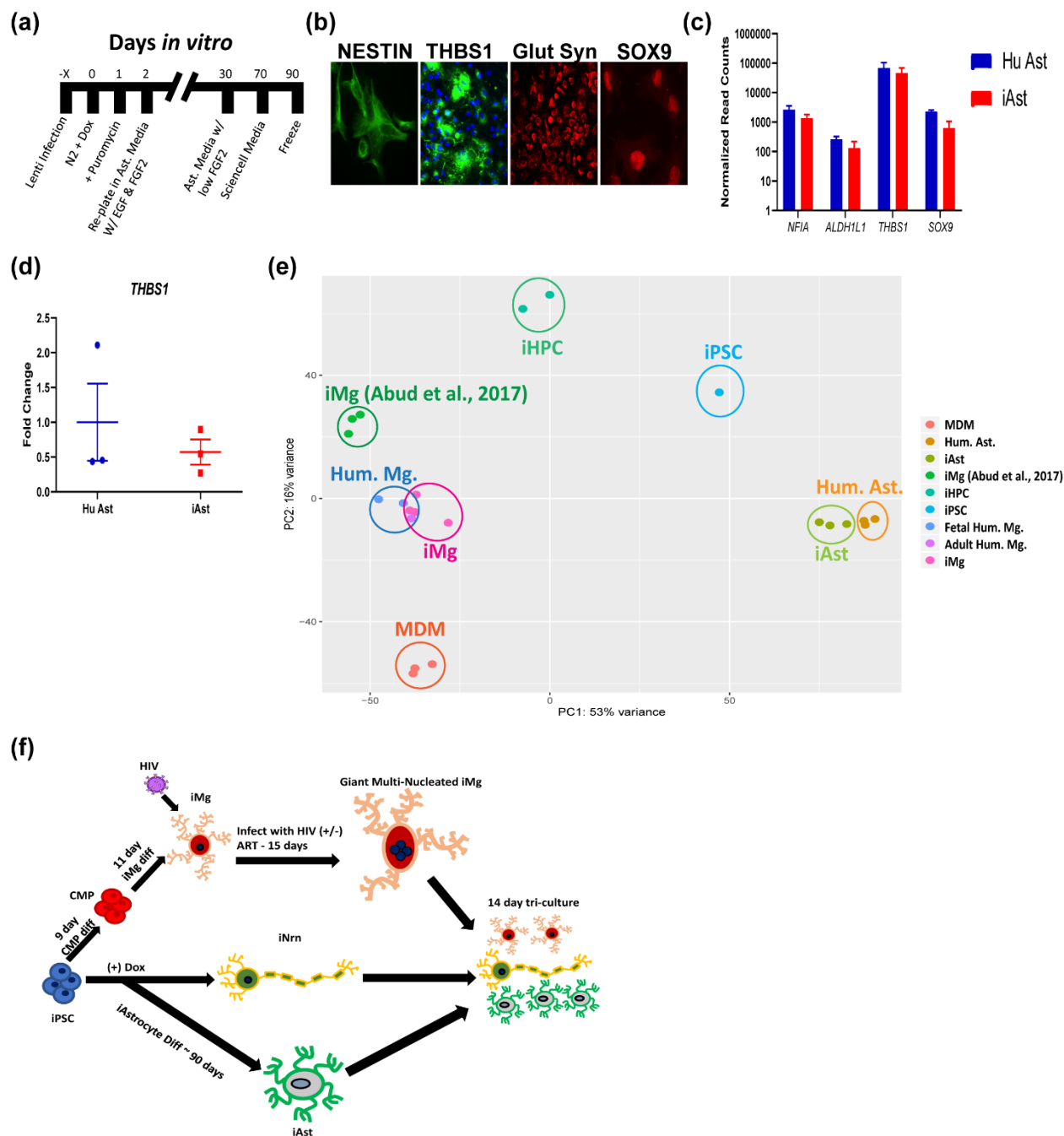
Figure 3: Generation and characterization of iAst and formation of tri-cultures

(a) Timeline for iAstrocyte differentiation. (b) Immunostaining for the Astrocyte specific markers: Nestin, Thrombospondin-1, Glutamine Synthetase, and SOX9. (c) Bulk RNAseq normalized read counts of select astrocyte specific genes from primary human astrocytes and iAst. n=3 cell lines, Benjamini-Hochberg, FDR 0.01, error bars represent SEM. (d) qRT-PCR validation for expression of *THBS1* in Hu Ast and iAst. Probe normalized to *GAPDH* expression. n=3 cell lines, two-tailed t test, error bars represent SEM. (e) PCA for monocyte-derived macrophages, iMicroglia, primary human astrocytes, and iAstrocytes, and (Abud et al., 2017) iMg, iPSC, iHPC, and primary human microglia. Each dot represents a bulk RNAseq sample. MDM - monocyte-derived macrophage; Hum. Ast. – primary fetal human astrocytes; iHPC – induced hematopoietic progenitor cells. iPSC, iHPC, Hum. Mg., iMg (Abud et al., 2017) samples were all retrieved from (Abud et al., 2017). (f) Flowchart for differentiations into iMg, iAst, and iNrn and combination into tri-culture ± HIV infection and ART.

11

212 **iNeurons were produced utilizing the NGN2 differentiation protocol**

213   We utilized a published NGN2 protocol (Zhang et al., 2013) to generate a homogenous

214 population of glutamatergic, forebrain-like excitatory neurons (Figure 3-figure supplement 1a

215 and 1b). Symptoms of HAND include loss of working memory, fine motor skills, and executive

216 function (Kathryn A. Lindl, Marks, Kolson, & Jordan-Sciutto, 2010; Saylor et al., 2016). Several of

217 these functions are controlled by the prefrontal cortex and hippocampus, where most neurons

218 are excitatory, glutamatergic neurons (Fuster, Bodner, & Kroger, 2000; Masterman & Cummings,

219 1997; Miller, 2000). We confirmed these neurons generate synapses (Figure 3-figure supplement

220 1c).

221

222 **iAstrocytes exhibit similar gene and protein expression as immature primary Astrocytes**

223   We noticed that by day 2 of the NGN2 differentiation, the cells took on a neural precursor-

224 like phenotype, expressing the neural progenitor markers Nestin and NCAM (Lendahl,

225 Zimmerman, & McKay, 1990; Marmur et al., 1998), and the astrocyte marker SOX9 (Kang et al.,

226 2012) (Figure 3-figure supplement 2a). Since neural progenitors can differentiate into astrocytes

227 *in vivo*, we attempted to shift the neural differentiation at day 2 from neurons to astrocytes by

228 removing the NGN2-inducing agent doxycycline, and adding FGF-2, EGF, and FBS to promote

229 astrocyte differentiation (Figure 3a). After 90 days, a homogenous-appearing population of iAst

230 were produced (Figure 3b). Bulk RNAseq revealed similar expression of several key genes for

231 immature astrocytes between iAst and primary, fetal human astrocytes (Hu Ast) (Figure 3c and

232 3e). qRT-PCR validation of *THBS1* confirmed no difference in expression Hu Ast and iAst (Figure

233 1d). The overall gene expression profile of the iAstrocytes is similar to fetal human primary

234 astrocytes (Figure 3e). We confirmed several of these genes at the protein level, including Nestin,

235 Glutamine Synthetase, THBS1 and SOX9 (Figure 3b), with 84.5 ± 22.9% expressing SOX9, 97.4 ±

236 2.3% expressing Nestin, 91.3 ± 2.4% expressing Glutamine Synthetase, and 46.5 ± 24.8%

237 expressing THBS1, an important protein in early synaptogenesis (Christopherson et al., 2005)

238 (Figure 3b); however, they did not express GFAP (Figure 3-figure supplement 2b). Additionally, in

239 mono-culture, they do not express the conventional glutamate transporter *GLT-1* or *GLAST*

240 (Figure 3-figure supplement 2b and 2c). Although in tri-culture, scRNAseq showed expression of

12

241 *GLT-1* (Figure 3-figure supplement 2e), which was not found in bulk RNAseq at the mono-culture

242 stage. Neuronal activity regulates GLT-1 in astrocytes (Awabdh et al., 2016; Perego et al., 2000;

243 Swanson et al., 1997), suggesting the iAst have a more *in vivo*-like phenotype when in the more

244 physiologically relevant tri-culture.

245

246 **iAst respond to HIV-induced cytokines produced by the iMg**

247 We also exposed the iAst in mono-culture to the most highly expressed cytokines in the

248 HIV-infected iMg, to determine if the cytokines produced by infected iMg can elicit an

249 inflammatory response in the iAst. We exposed the iAst to IL-1b and IL-8 at 10ng/mL for eight

250 hours and then analyzed the supernatants on the same six-cytokine panel. We found that, of the

251 six cytokines tested, the iAst produced increased amounts of IL-1a (Figure 2-figure supplement

252 5b), suggesting that the iMicroglia can elicit an inflammatory response in the iAst. In addition, it

253 is interesting that IL-1a was released given its role in producing A1 astrocytes (Liddelow et al.,

254 2017).

255

256 **The HiPSC-derived tri-culture is sustainable with iAst and iMg derived from novel**

257 **differentiation protocols**

258 In order to study the cell-cell interactions during HIV infection and subsequent

259 antiretroviral treatment (ART), we developed a novel tri-culture system of HiPSC-derived

260 microglia (iMg), neurons (iNrn), and astrocytes (iAst) by separately differentiating each cell type,

261 infecting the iMg (± ART), then co-plating the different populations into a carpet culture for

262 analysis. The tri-culture is able to survive for at least 2 weeks (Figure 3f).
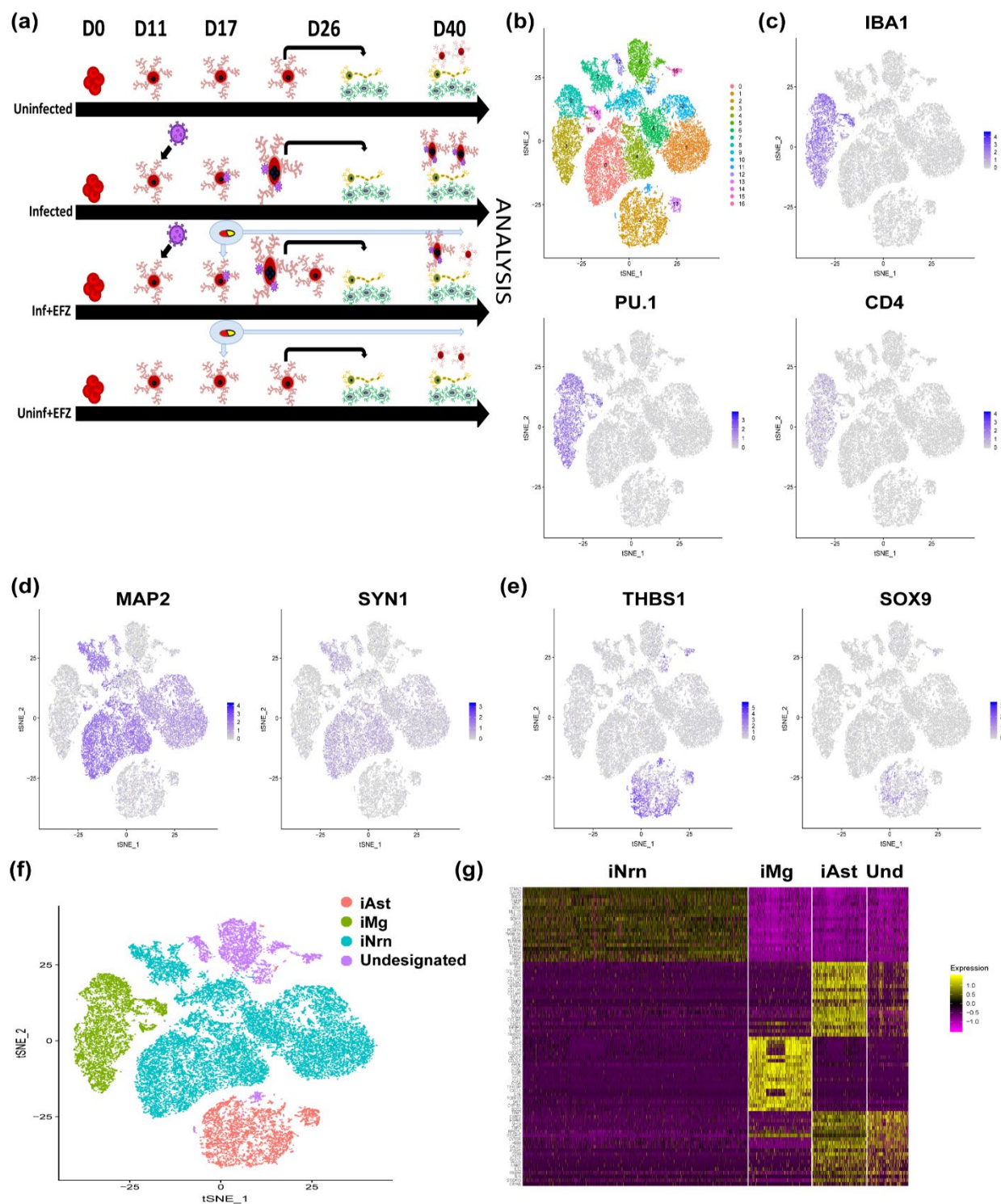
Figure 4: scRNAseq identified each of the three cell types in all four conditions

(a) Timeline from start of CMP differentiation through tri-culture for the four conditions. (b) t-SNE of unbiased clustering of combined scRNAseq from all four conditions. (c-e) expression patterns of cell type specific markers for microglia (c), neurons (d), and astrocytes (e). (f) t-SNE clustering by cell type based on cell type specific marker expression. One cluster did not align with any of the three cell types by the expression patterns chosen in (c-e). (g) Heat map of top 20 genes expressed in each cell type reveals the undesignated cluster of cells to be similar to iAst expression profile, suggesting they may be immature iAst.

scRNAseq identified each of the three cell types in all four conditions

Next, we studied the cell types' reactions in a more physiologically relevant tri-culture. To create the tri-culture, we began the iNrn differentiation, added the iAst at D5 of the iNrn differentiation, after the Ara-C had been removed, and added the iMg at D7 of the iNrn differentiation. The tri-culture was maintained for an additional 14 days, to D21 of the iNrn differentiation (Figure 4a). To assay gene expression changes in each of the three cell types during HIV infection ± EFZ, we conducted scRNAseq on the tri-culture under four conditions: Uninf, Inf, Inf+EFZ, and Uninf+EFZ (Figure 4a). Cells were sequenced from the Uninf (n=6,564), Inf (n=7,431), Inf+EFZ (n=7,111), and Uninf+ EFZ (n=10,071) conditions. All conditions were then aggregated and initially analyzed through the cellranger pipeline (10x Genomics, v.3.0.1). Secondary analysis was performed using the Seurat package in R. We generated 16 unbiased clusters (Figure 4b). First, we separated the clusters by cell type, then broke down each cell cluster by condition. We assigned clusters to one of the three cell types by expression of several key genes: iMg by expression of *IBA1*, *PU.1*, and *CD4*; iNrn by expression of *MAP2* and *SYN1*; and iAst by expression of *THBS1* and *SOX9* (Figures 4c-4e). There were four clusters (cluster 5, 10, 12, and 13) that did not fit into any of the three cell types by expression of the chosen markers (Figure 4b and 4f). To determine what the fourth cell type might represent, we examined the expression of the top 20 genes in each of the 4 cell types (Figure 4g). The gene expression pattern of the undesignated cells best matched the iAst, but scRNAseq did not capture expression of THBS1 or SOX9, suggesting these cells represent less mature versions of the iAst. Hence, they were excluded from further analysis (Figure 5a). We then separated each cell type by condition (Figure 5b).
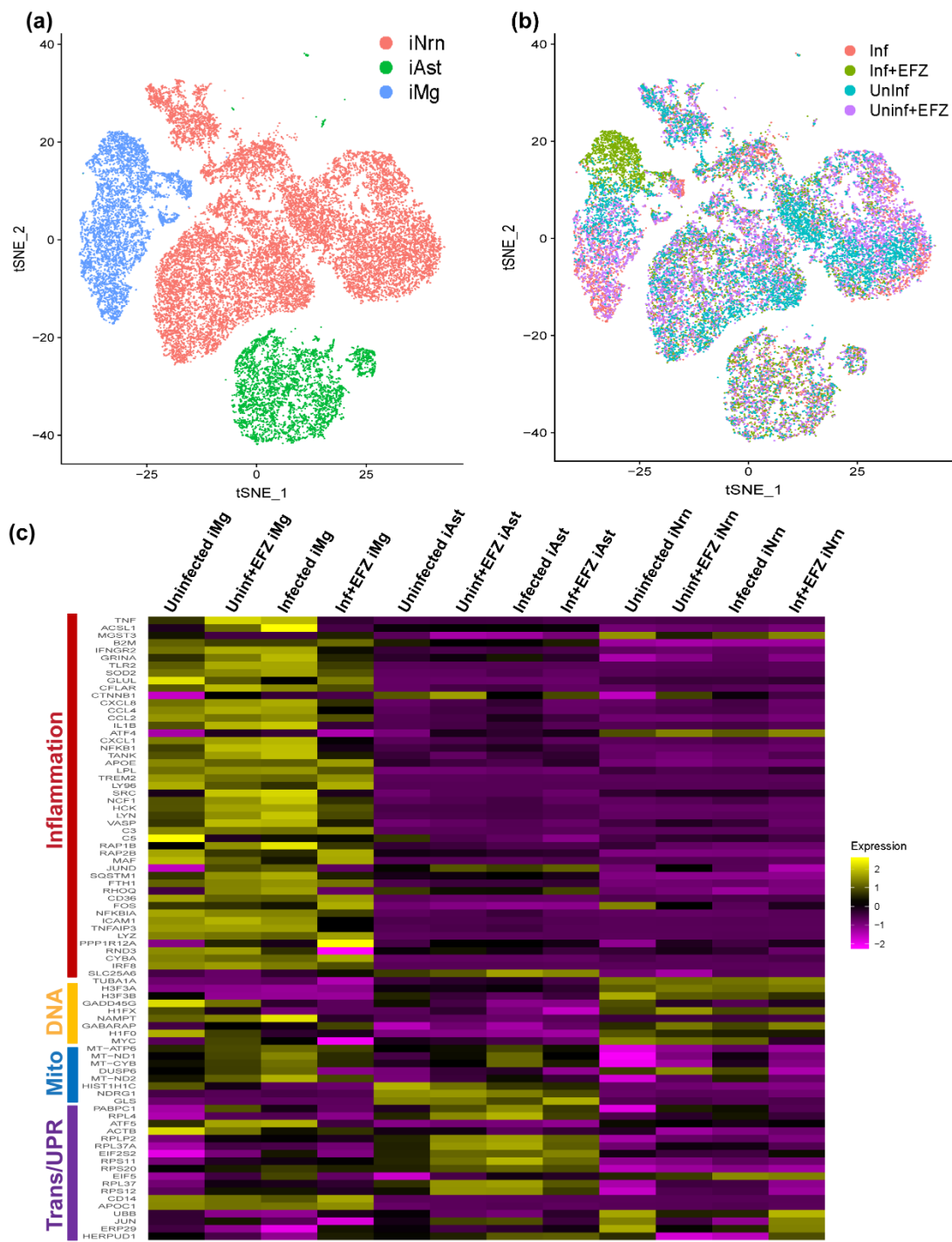
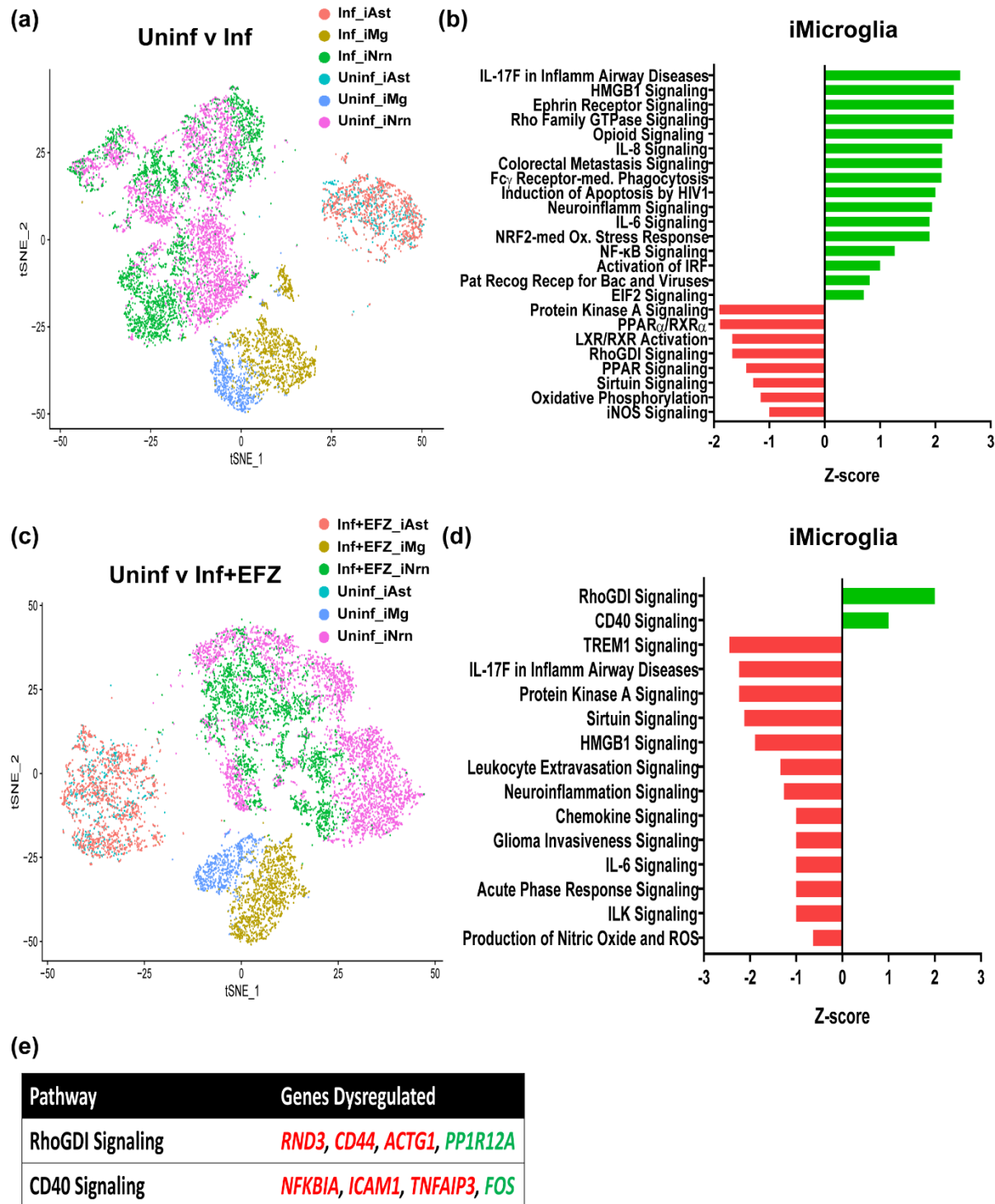**Figure 5: iMg exhibit the largest inflammatory response by gene expression among the three cell types in tri-culture**

(a) t-SNE plot of all cells from all conditions excluding the undesignated cluster. (b) t-SNE from (a) broken down by condition. (c) Heatmap of inflammation, DNA accessibility, mitochondria, and translation/UPR related genes in iAst, iNrn, and iMg in all four conditions: Uninf, Uninf+EFZ, Inf, Inf+EFZ.

iMg exhibit the largest inflammatory response by gene expression

After the scRNAseq was separated by cell type (Figure 5a) and condition (Figure 5b), We examined a panel of inflammation, DNA accessibility, mitochondria, and translation/UPR-related genes to determine which of the three cell types had the greatest changes in relevant gene expression (Figure 5c). The iAst had the most prominent change in translation and UPR related genes, with increased expression of several ribosomal genes and *EIF2S2*, a subunit of EIF2, in the Inf condition compared to Uninf. Whereas, the iNrn had the largest increases in DNA accessibility genes, including several histone-related genes. Not surprisingly, the iMg population showed the highest expression of inflammatory and mitochondria related genes. Inf iMg had increased expression of several inflammatory cytokine genes, including *CXCL8* and *IL-1b*. This corroborates with the increased production if IL-8 and IL-1b in infected iMg in mono-culture. The Inf+EFZ iMg had lower expression levels than Inf iMg for these genes, again corroborating with the mono-culture cytokine production. Although, the Inf+EFZ iMg had increased expression of the inflammatory genes *FOS* and *APOE*, compared to control. These results suggest that the iMg are mostly responsible for the inflammatory response during infection ± EFZ; however, there are distinct responses ± EFZ. To further investigate the differences, we next performed pairwise comparisons of each cell type across all four conditions.

(a) Uninf v Inf

Legend: Inf_iAst, Inf_iMg, Inf_iNrn, Uninf_iAst, Uninf_iMg, Uninf_iNrn

(b) iMicroglia

Pathways (top to bottom):
IL-17F in Inflamm Airway Diseases
HMGB1 Signaling
Ephrin Receptor Signaling
Rho Family GTPase Signaling
Opioid Signaling
IL-8 Signaling
Colorectal Metastasis Signaling
Fcγ Receptor-med. Phagocytosis
Induction of Apoptosis by HIV1
Neuroinflamm Signaling
IL-6 Signaling
NRF2-med Ox. Stress Response
NF-κB Signaling
Activation of IRF
Pat Recog Recep for Bac and Viruses
EIF2 Signaling
Protein Kinase A Signaling
PPARα/RXRα
LXR/RXR Activation
RhoGDI Signaling
PPAR Signaling
Sirtuin Signaling
Oxidative Phosphorylation
iNOS Signaling

X-axis: Z-score (-2 to 3)

(c) Uninf v Inf+EFZ

Legend: Inf+EFZ_iAst, Inf+EFZ_iMg, Inf+EFZ_iNrn, Uninf_iAst, Uninf_iMg, Uninf_iNrn

(d) iMicroglia

Pathways (top to bottom):
RhoGDI Signaling
CD40 Signaling
TREM1 Signaling
IL-17F in Inflamm Airway Diseases
Protein Kinase A Signaling
Sirtuin Signaling
HMGB1 Signaling
Leukocyte Extravasation Signaling
Neuroinflammation Signaling
Chemokine Signaling
Glioma Invasiveness Signaling
IL-6 Signaling
Acute Phase Response Signaling
ILK Signaling
Production of Nitric Oxide and ROS

X-axis: Z-score (-3 to 3)

(e)

Pathway	Genes Dysregulated
RhoGDI Signaling	*RND3*, *CD44*, *ACTG1*, *PP1R12A*
CD40 Signaling	*NFKBIA*, *ICAM1*, *TNFAIP3*, *FOS*

Figure 6: iMg activate RhoGDI and CD40 in response to HIV infection with EFZ treatment

(a) t-SNE plot of Uninf and Inf conditions. (b) Ingenuity pathway analysis of iMg between Uninf and Inf conditions. Uninf is baseline. Benjamini-Hochberg FDR 0.05, Fisher's exact <0.05, z-score cutoff ± 0.5. (c) t-SNE plot of Uninf and Inf+EFZ conditions. (d) Ingenuity pathway analysis of iMg between Uninf and Inf+EFZ conditions. Uninf is baseline. Benjamini-Hochberg FDR 0.05, Fisher's exact <0.05, z-score cutoff ± 0.5. (e) Specific genes dysregulated that are involved in the RhoGDI and CD40 pathways in Inf+EFZ iMg compared to Uninf iMg. Red genes are downregulated. Green genes are upregulated.

18

Inflammatory pathways and EIF2 signaling were consistently dysregulated among all three cell types during infection, but iMg were the most affected

We first compared the Inf condition to Uninf. Several inflammatory pathways were highly activated in Inf iMg compared to Uninf iMg, including Il-8 and NF-κB signaling. One of the top pathways dysregulated in Inf iMg compared to Uninf was the EIF2 pathway (Figures 6b). EIF2 signaling is involved in the UPR and, more broadly, the ISR (Cui, Li, Ron, & Sha, 2011; Janssens, Pulendran, & Lambrecht, 2014; Walter & Ron, 2011). The EIF2 pathway was not only dysregulated in iMg, but also was consistently increased in the iAst and iNrn (Figure 6-figure supplement 1a and 1b). However, only iMg had increased expression of *ATF4*, the downstream transcription factor of the PERK arm of the ISR, which leads to increased cytokine production (Masuda, Miyazaki-Anzai, Levi, Ting, & Miyazaki, 2013) in Uninf v Inf (Figure 5c). Previously, we have shown that the PERK arm of the ISR is activated in neurons and astrocytes from human brain samples with HAND (C. Akay et al., 2012; K. A. Lindl, Akay, Wang, White, & Jordan-Sciutto, 2007).

Infection+EFZ had distinct increased activation of RhoGDI and CD40 pathways

We next compared Uninf to Inf+EFZ, expecting to see a dampened immune response compared to Inf. Many of the top affected pathways in Inf iMg were related to inflammation; however, there does seem to be a stark difference between Inf iMg and Inf+EFZ iMg (Figures 6b and 6d). The Inf+EFZ had a much milder inflammatory reaction, where RhoGDI and CD40 signaling were the only upregulated pathways compared to Uninf iMg (Figure 6d and 6e). RhoGDI negatively regulates Rac, which functions in multiple inflammation pathways (Wilkinson & Landreth, 2006), and CD40 activates NF-κB signaling (D'Aversa et al., 2008; Homig-Holzel et al., 2008). A milder inflammatory response corroborates well with lesser disease severity seen in HAND patients who are taking ART (Saylor et al., 2016).

The scRNAseq data suggest the microglia were most affected by the infection ± EFZ, with major changes to EIF2 signaling, inflammatory, oxidative damage, and phagocytic gene pathways. However, the distinct activation of RhoGDI and CD40 in the Inf+EFZ condition suggests the combination of Inf+EFZ creates a distinct effect. We thus further investigated the effects of Inf+EFZ treatment compared to Inf and Uninf+EFZ treatment.

355

356 **Inf+EFZ has an attenuated, but distinct inflammatory response compared to Inf and Uninf+EFZ**

357   Inf iMg had increased activity in several inflammatory pathways including IL-6 signaling,

358 neuroinflammation signaling, and Fcγ receptor-mediated phagocytosis compared to Inf+EFZ

359 (Figure 6-figure supplement 2a and 2b), suggesting the Inf+EFZ had an overall lower immune

360 response. However, the EIF2 signaling pathway, part of the UPR, was lower in Inf iMg compared

361 to Inf+EFZ (Figure 6-figure supplement 2b).

362   We next compared Uninf+EFZ to Inf+EFZ (Figure 6-figure supplement 2c). EIF2 signaling

363 was increased in the Inf+EFZ iMg (Figure 6-figure supplement 2d), similar to the Inf and Inf+EFZ

364 comparison (Figure 6-figure supplement 2b). However, inflammatory pathways including

365 neuroinflammation and ROS/iNOS signaling were higher in Uninf+EFZ compared to Inf+EFZ iMg

366 (Figure 6-figure supplement 2d). Inf+EFZ iMg again had increased activation of the CD40 and

367 RhoGDI pathways (Figure 6-figure supplement 2d and 2e) compared to Uninf+EFZ, suggesting a

368 distinct inflammatory response with the combination of infection and EFZ treatment.

369   iAst had activation of the neuroinflammation and RhoGDI signaling pathways in Inf+EFZ

370 than Uninf+EFZ (Figure 7-figure supplement 1e). These results show a stark difference in

371 responses to EFZ treatment alone and EFZ treatment with infection, suggesting combinatorial

372 and probably interacting effects of infection and EFZ treatment.

20
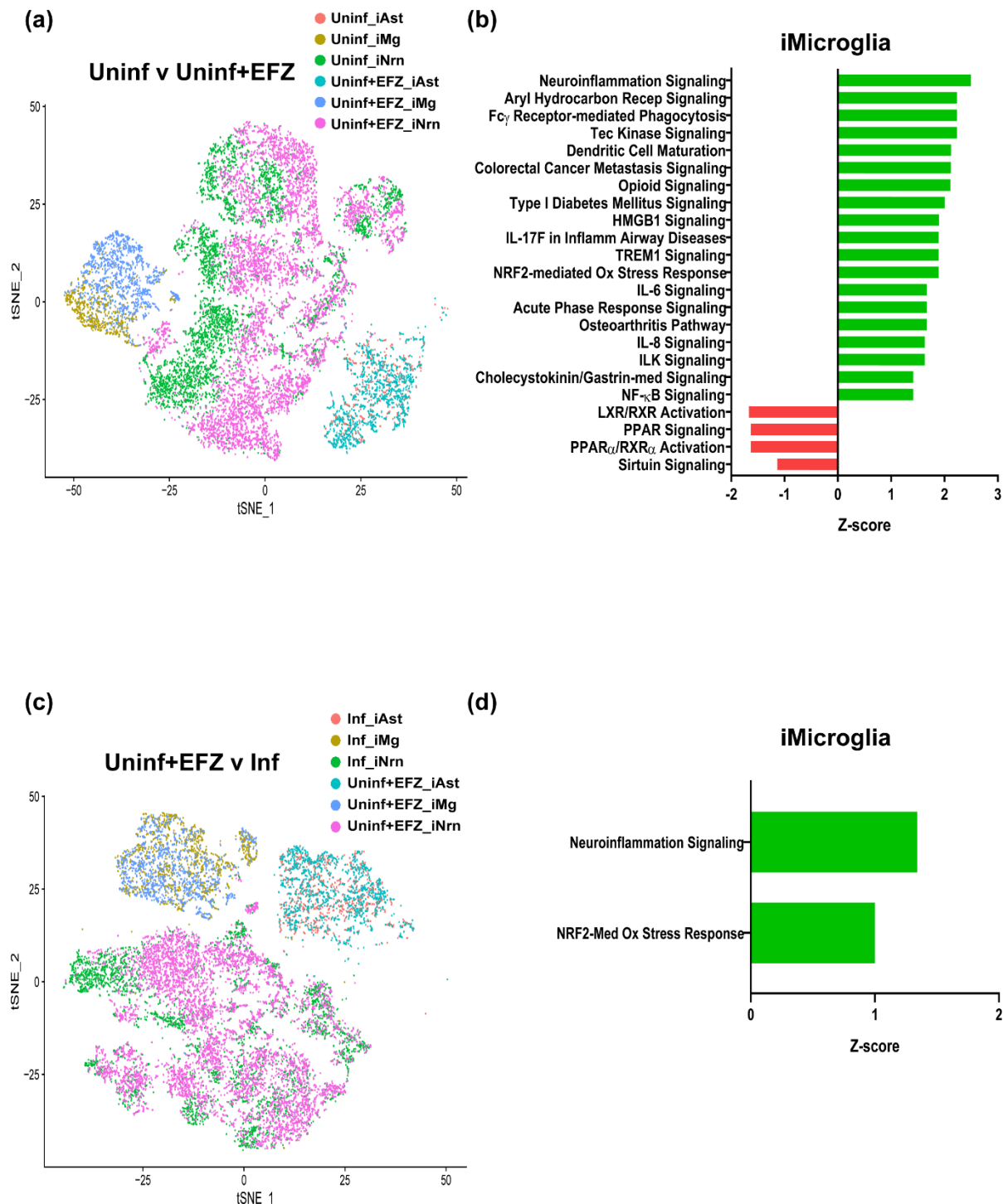
Figure 7: EFZ treatment alone elicits comparable response as infection

(a) t-SNE plot of Uninf and Uninf+EFZ conditions. (b) Ingenuity pathway analysis of iMg between Uninf and Uninf+EFZ conditions. Uninf is baseline. Benjamini-Hochberg FDR 0.05, Fisher's exact <0.05, z-score cutoff ± 0.5. (c) t-SNE plot of Uninf+EFZ and Inf conditions. (d) Ingenuity pathway analysis of iMg between Uninf+EFZ and Inf conditions. Uninf+EFZ is baseline. Benjamini-Hochberg FDR 0.05, Fisher's exact <0.05, z-score cutoff ± 0.5.

21

381   **Uninf+EFZ creates an inflammatory response similar to Inf**

382   Inf+EFZ had a starkly different response than Uninf+EFZ. So, we further investigated the

383   effect of EFZ treatment alone compared to Uninf and Inf treatments. ART can be used as a

384   preemptive treatment against HIV infection; however, it has various inflammatory and

385   neurotoxic side effects (Cagla Akay et al., 2014; Robertson, Liner, & Meeker, 2012). How ART

386   affects different cell types in co-culture has not been explored. We compared Uninf+EFZ to the

387   Uninf (Figures 7a, 7b, and Figure 7-figure supplement 1a and 1b) and Inf (Figures 7c, 7d, Figure

388   7-figure supplement 1c and 1d) and found a surprisingly similar gene expression profile to the Inf

389   condition, especially in the iMg and iAst. The pairwise comparison of Uninf and Uninf+EFZ

390   revealed multiple inflammatory pathways increased in Uninf+EFZ iMg, with neuroinflammation

391   signaling as the most activated pathway (Figure 7b). Several of the other pathways activated,

392   including IL-6 and IL-8 signaling, were also found in the Uninf v Inf comparison (Figure 6b). EIF2

393   signaling was increased in Uninf+EFZ iNrn compared to Uninf (Figure 7-figure supplement 1b),

394   similar to Inf iNrn (Figure 6-figure supplement 1b). EIF2 signaling was not increased in the iAst,

395   unlike in the Inf comparison, and there was a reversal for sirtuin signaling with inhibition in the

396   Uninf+EFZ versus Uninf (Figure 7-figure supplement 1a), suggesting Uninf+EFZ elicits a similar,

397   but not identical inflammatory response as Inf.

398   We found iMg had higher activation of neuroinflammation signaling and NRF2-mediated

399   oxidative stress response in Inf compared to Uninf+EFZ (Figures 7c and 7d). iNeurons had higher

400   oxidative phosphorylation activation; however, we found no statistically significant changes in

401   any canonical pathways in iAst between the conditions (Figure 7-figure supplement 1c and 1d),

402   suggesting an inflammatory response by iMg and change in mitochondria function in neurons in

403   response to HIV infection of the former.

404   Infection, EFZ treatment alone, and infection with EFZ treatment all induced distinct

405   responses not only across conditions, but also across cell types within conditions. These data

406   reveal a potential downside to pre-emptive ART use and suggest that the inflammatory response

407   from Infected to Inf+EFZ to Uninf+EFZ is not a linear regression as one might expect, but rather

408   three distinct responses. We further investigated these gene pathway changes by testing for

409   cytokine production and phagocytic abilities.

22

410
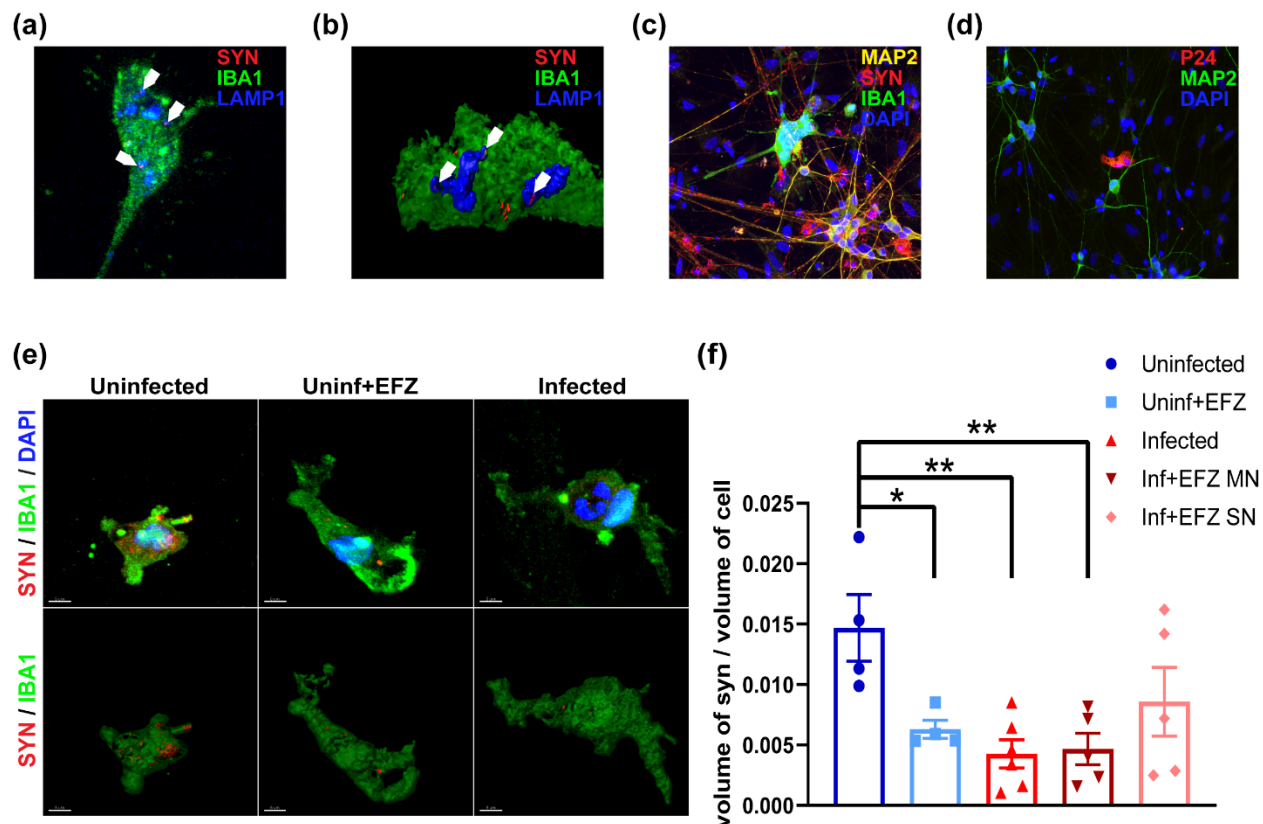
Figure 8: HIV-infected iMicroglia have reduced synaptophagocytosis, which is ameliorated by EFZ treatment

(a&b) Immunostaining (a) and surface reconstruction of a side view (b) of iMg in an iNrn co-culture displaying synaptic phagocytosis by co-localization of synaptophysin+ (red) puncta within LAMP1+ (blue) lysosomes in IBA1+ (green) iMg. (c) Giant multi-nucleated IBA1+ (green) iMg potentially interacting with synaptophysin+ (red) synapses on MAP2+ (yellow) dendrites. (d) Multi-nucleated iMg, but not MAP2+ (green) iNrn or iAst, are P24+ (red) in the tri-culture after 14 days. (e) Representative surface reconstructions of synaptophysin signal (red) within IBA1+ (green) iMg in the Uninf, Uninf+EFZ, and Inf tri-cultures. SN-single nucleated. MN-multinucleated. Scale bar represents 5μm. (f) Synaptophagy is significantly decreased in infected iMg ± EFZ and uninfected iMg + EFZ compared to control. n=4 (4 Uninf, 4 Uninf+EFZ, 6 Inf, 5 Inf+EFZ) differentiations, one-way ANOVA, Dunnett's post hoc analysis, $p<0.05$, error bars represent SEM.

Synaptophagocytosis is impaired in Inf, Inf+EFZ iMg, and Uninf+EFZ iMg

We interrogated the ability of iMg to phagocytose synaptic material to further explore the possible differences in the responses to infection ± EFZ and EFZ treatment alone. Fcγ receptor mediated phagocytosis pathway was activated in the Inf iMg as well as the Uninf+EFZ iMg compared to Uninf iMg (Figures 6b and 7b). Aberrant synaptophagy by microglia has been implicated in multiple neurological disorders including Alzheimer's and Frontotemporal dementia (Hong et al., 2016; Lui et al., 2016). Many antiretrovirals, including Efavirenz, have reported neurotoxic effects (Ciccarelli et al., 2011; Robertson et al., 2012) and reduce

23

431 phagocytosis (Giunta et al., 2011). In addition, HIV-infected macrophages and uninfected

432 macrophages exposed to HIV display decreased phagocytic capabilities, specifically through the

433 Fcγ receptor-mediated pathway and not complement, due to Nef and Tat inhibiting endocytosis

434 (Debaisieux et al., 2015; Giunta et al., 2008; Mazzolini et al., 2010), but human microglia

435 synaptophagocytosis has never been tested.

436   In order to determine their ability to phagocytose synapses, we generated tri-culture of

437 the iMg with the iNrn and iAst and examined them 14 days after adding the iMg (Figure 4a). The

438 cultures were subjected to immunofluorescence for IBA1, the lysosomal marker LAMP1, and the

439 pre-synaptic marker SYN1. We found colocalization of SYN1 in the LAMP1+ lysosomes of the iMg

440 (Figure 8a and 8b), suggesting that the iMg phagocytize synaptic material. We confirmed that

441 iMg are in contact with iNrns (Figure 8c), and importantly, only the iMg are infected as only they,

442 and not the iNrns (Figure 8d) or iAstrocytes, show P24 immunofluorescence. Additionally, RT

443 activity confirmed that the iMg in the infected condition remain productively infected (Figure 9a).

444 We were also able to delineate infected from uninfected iMg in the Inf+EFZ condition by multi-

445 nucleation (Figures 2c, 2d, and Figure 8-figure supplement 1a).

446   We utilized confocal imaging and 3D reconstruction to measure the total synaptic volume,

447 as indicated by synaptophysin immunofluorescence, within the iMg. The Inf iMg showed reduced

448 synaptophagocytosis compared to Uninf iMg. In addition, in the Inf+EFZ condition, the infected

449 (multinucleated) have reduced phagocytosis; however, the uninfected (single-nucleated) iMg in

450 the Inf+EFZ condition trended lower but was not statistically significant. Lastly, Uninf+EFZ

451 condition iMg also had impaired synaptophagocytosis (Figure 8e and 8f). Multiple factors from

452 the virus itself, the immune response, and the effects of antiretrovirals are acting on the iMg

453 during HIV infection. All these factors may play a role in reducing synaptic phagocytosis and

454 warrant future study.

455   While the Fcγ receptor-mediated phagocytosis pathway was activated in Inf iMg, several

456 of the genes dysregulated including: *ACTB*, *ACTR3*, *ARPC2*, *FYB1*, *RAC1*, and *VASP* (data not

457 shown), were associated with the nascent phagosome and phagosome formation, which is

458 targeted by Nef in impairing phagocytosis (Dirk et al., 2016; Mazzolini et al., 2010), suggesting a

459 compensatory increase in gene expression for genes associated with the target for Nef, early

460 endocytosis. This finding may partially explain the apparent paradox in increased pathway

461 activity of Fcγ receptor-mediated phagocytosis, but impaired phagocytosis in Inf iMg.

462   To confirm that differences in apparent iMg synaptophagy are not secondary to reduced

463 numbers of synapses overall in a given culture condition, we also measured local and random (50

464 μm radius areas with no iMg) synapse density to ensure the uninfected microglia were not in a

465 more synapse dense area (Figure 8-figure supplement 2a and 2b). In fact, there was no significant

466 difference in iMg-proximal or random synapse density across all conditions (Figure 8-figure

467 supplement 2c and 2d). This finding aligns with previous studies that demonstrate inhibition of

468 phagocytosis by viral proteins Tat and Nef in both infected and uninfected macrophages,

469 (Debaisieux et al., 2015; Giunta et al., 2008; Mazzolini et al., 2010), and is also consistent with

470 ART-related impairment of phagocytosis (Giunta et al., 2011).

25
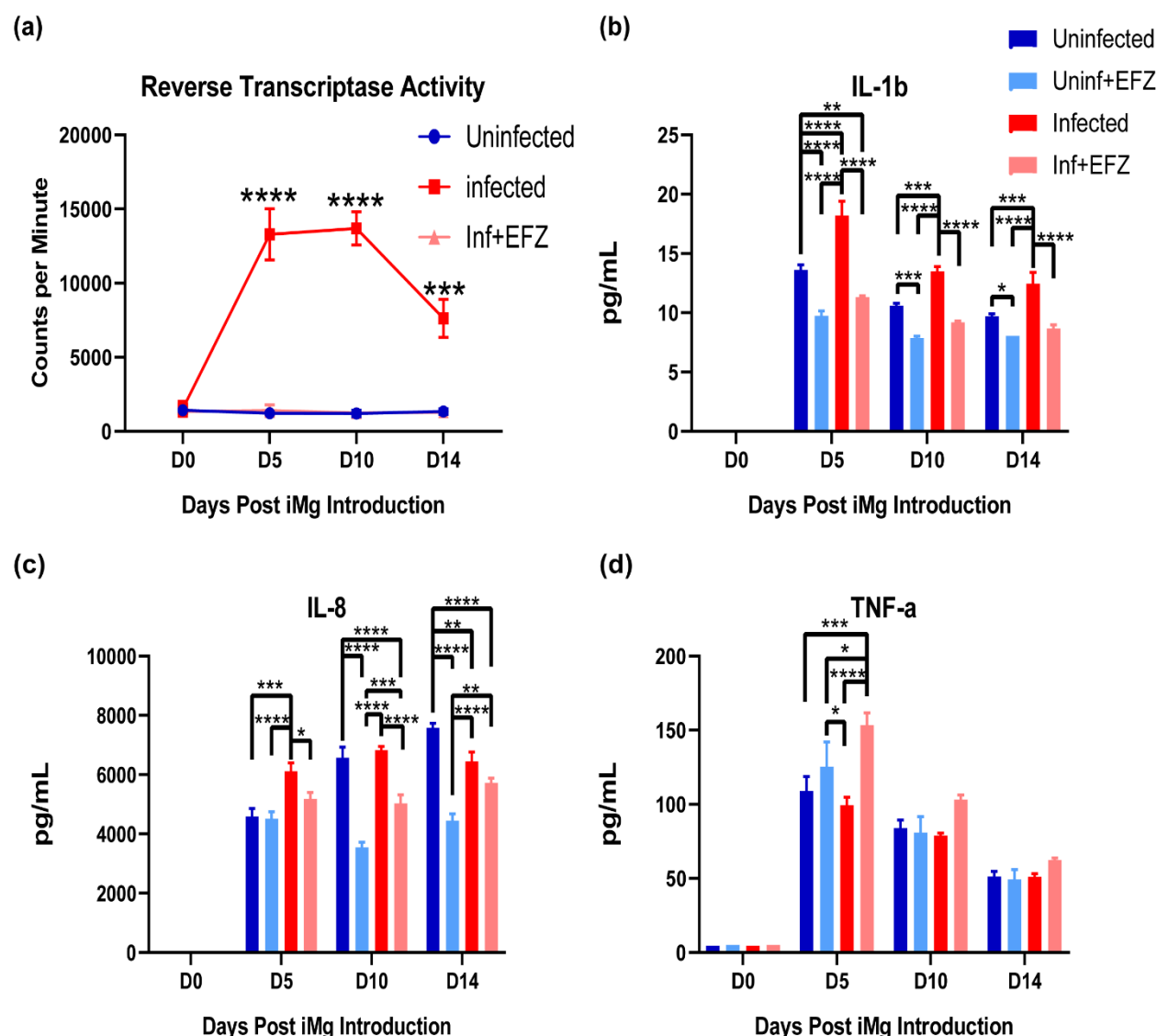
Figure 9: Inf+EFZ mitigates IL-1b and IL-8 production, but increases TNFa production

(a) Reverse transcriptase activity of Uninf, Inf, and Inf+EFZ tri-culture shows continual productive infection. n=3 infections, one-way ANOVA, Dunnett's post hoc analysis, ***p<0.001; ****p<0.0001, error bars represent SEM. (b-d) Cytokine analysis of Uninf, Uninf+EFZ, Inf, and Inf+EFZ iMg displays increase in IL-1b (b) and IL-8 (c) production in the Inf tri-culture, and Inf+EFZ had increased TNFa (d). n=3 infections, two-way ANOVA, Tukey's post hoc analysis, *p<0.05; **p<0.01; ***p<0.001; ****p<0.0001, error bars represent SEM.

EFZ reduces the production of IL-8 and IL-1b by infected iMg, but enhances TNFa

Lastly, we compared cytokine production between each condition in tri-culture. Starting at the time of iMg addition, we collected supernatant every 5 days until day 14 of tri-culture. IL-8 and IL-1b were significantly increased in the infected tri-culture compared to uninfected control. IL-1b remained increased over uninfected; however, IL-8 decreases by day 10 (Figure 9b and 9c). Unlike in mono-culture, the Inf+EFZ condition had reduced cytokine production of IL-8

26

485   and IL-1b compared to uninfected. Uninf+EFZ had the lowest levels of cytokine production across

486   all the groups (Figure 9b-9d). In addition, there was no increase in TNFa in the Inf tri-culture;

487   however, the Inf+EFZ condition did have increased TNFa (Figure 9d). The Inf and Inf+EFZ tri-

488   cultures also did not exhibit increases in IL-6 or IL-10, similar to our mono-culture findings (Figure

489   2-figure supplement 3c and 3d). These data combined with the scRNA data suggest there are

490   distinct influences on the inflammatory response during infection alone and infection with EFZ.

491   iMg in the Inf condition exclusively had increased expression of *IL-8* and *IL-1b* genes (Figure 5c).

492   In addition, IL-8 and NF-κB signaling were activated only in iMg in the Inf condition by scRNAseq

493   (Figure 6b) Interestingly, TNFa regulates *AP-1* (*FOS*) (Clark, Vagenas, Panesar, & Cope, 2005), a

494   CD40 signaling pathway gene that is upregulated in Inf+EFZ iMg when compared to the Uninf

495   (Figures 5c and 6d). These results further suggest distinct inflammatory reactions from Inf and

496   Inf+EFZ that are mostly caused by the iMg.

Discussion

We describe, to our knowledge, the first HiPSC tri-culture model to investigate the interdependent and individual roles of microglia, astrocytes, and neurons in the context of HIV infection. In recent years, there have been several new differentiation protocols for these cell types (Abud et al., 2017; Santos et al., 2017; Zhang et al., 2013) and several iPSC/primary cell co-cultures that have studied various neurological disorders (Lin et al., 2018; Park et al., 2018). This model goes one step further, exploring gene expression changes with scRNA sequencing in the context of viral infection and relevant drug treatments to begin to unfurl a particularly difficult disease to study.

Although there are missing components to this model, it is still able to recapitulate several findings *in vivo*, such as increases in IL-8 and IL-1β production and EIF2 signaling (C. Akay et al., 2012; Ginsberg et al., 2018; Tatro et al., 2014). It has also discovered novel changes that require further investigation but could lead to advancements in therapeutics. This system allowed us to identify sirtuin pathway dysregulation, which has been implicated in aging and Alzheimer's, but not HAND (Cho et al., 2015; Jesko, Wencel, Strosznajder, & Strosznajder, 2017).

We were also able to show that the microglia seem to be the main culprit in the initial response to HIV infection; however, at least within the two-week period of this study, iMg infection does not lead to aberrant phagocytosis of synapses. This falls in line with previously reported impaired phagocytosis by HIV-infected or exposed macrophage (Debaisieux et al., 2015; Mazzolini et al., 2010). With Nef and Tat targeting early stages of the phagocytosis, and most of the genes dysregulated in the Fcγ receptor-mediated phagocytosis target early endocytosis, it is likely that the increased pathway activation is a compensation mechanism. Infection with HIVΔNef could confirm this.

In addition, we discovered a starkly different immune response at the gene and functional level in Inf versus Inf+EFZ. CD40 and RhoGDI activation could be controlled by the increased production of TNFa, that was only found in the Inf+EFZ condition. This persistent immune activation highlights the need for further studies into the role that antiretrovirals play in propagating the chronic inflammation seen in HIV patients today (Kolson, 2017; Saylor et al., 2016). The mitigated reaction we observed with EFZ treatment is consistent with human studies

526 showing a reduced severity of HAND with the widespread use of antiretroviral therapies (Saylor

527 et al., 2016), but also with its persistence despite control of viral load. Further, we revealed a

528 substantial immune response to EFZ treatment alone. This warrants further study as people take

529 ART as a preventative measure (Spinner et al., 2016).

530 HiPSC cultures are particularly useful for studying HIV neuropathology, since human

531 primary neuronal cells and postmortem tissue are limited in availability and not amenable to

532 molecular manipulation. In addition, HIV only infects human cells, rendering the interpretation

533 of results from animal models more convoluted. Hence, mechanistic studies of the influences of

534 HIV and ART on human neural cells are limited. This tri-culture system allows us to better study

535 the mechanisms of early HIV infection in the brain; however, there are caveats to this system

536 that must be considered. Each of the iPSC-derived cell types are similar to their *in vivo*

537 counterparts by gene and protein expression, as well as, function, but are not exact. In addition,

538 the iCells' gene expression profile at the end stage of differentiation is relatively immature and

539 more closely represents early stages of development *in vivo*. Our culture system allows

540 reductionist study of three key cell types over weeks but may be refined by inclusion of additional

541 cell types, and further optimization to model HAND in the adult setting.

542 This tri-culture has validated several findings in the field as well as produced multiple novel

543 findings for HIV neuropathology. However, this model is not restricted to HIV neuropathology

544 and can also be utilized to study other neurological disorders. This highly tractable, reductive

545 system can be genetically and pharmacologically modified at any stage. These differentiations

546 could also be used on patient-derived cells, creating a disease-relevant, patient-specific tri-

547 culture system. Similar cultures have been developed (Haenseler et al., 2017; Park et al., 2018),

548 but not to this complexity, as rapid a differentiation, or with a focus on viral infections. The tri-

549 culture can be another, instrumental tool in understanding the workings of complex neurological

550 disorders and in developing novel therapeutic strategies.

29

Materials and Methods

Human induced pluripotent stem cell lines

HiPSC lines for the iNrn and iAst were generously received from Herbert M. Lachman, MD., Einstein University, Bronx, New York. All lines were trained over to a feeder-free system with Stem MACS iPS-Brew XF media (Miltenyi Biotec 130-104-368). Lines were tested for mycoplasma using Lookout mycoplasma PCR detection kit (Sigma MP0035). iPSC lines for the iMg were cultured by the Human Pluripotent Stem Cell Core (CHOP).

iNeuron differentiation of iPSCs

iPSCs were transfected with two plasmids VSVG.HIV.SIN.cPPT.CMV.mNgn2.WPRE and VSVG.HIV.SIN.cPPT.CMV.rTTA.WPRE, produced by Marius Wernig (Stanford University) and packaged by the University of Pennsylvania Viral Vector Core. Cells were exposed to 1ug/mL polybrene (Sigma Aldrich TR-1003). Media is fully exchanged six hours after exposure. iPSCs are differentiated according to a previously published method (Zhang et al., 2013). In brief, after transfection, iPSCs were exposed to N2 media containing 5 mL N2 Supplement-B (Stemcell Technologies 07156), 0.5mL 55mM β-mercaptoethanol (Life technologies 21985-023), 0.5mL primocin (Invivogen ant-pm-2), BDNF (10ng/mL, peprotech 450-02), NT-3 (10ng/mL, peprotech 450-03), laminin (200ng/mL, Sigma L2020), and doxycycline (2ug/mL, Sigma D3072) in DMEM / F12 (Gibco 11320-033) for 24 hours (DIV0). Cells were then exposed to puromycin (5ug/mL, Sigma P9620) for 24 hours in the same N2 media (DIV1). iNeurons were re-plated 24 hours later (DIV2) to experiment appropriate plates coated with Matrigel GFR (Corning 354230). Cells were washed 2x in PBS and lifted with StemPro accutase (Thermo Fisher Scientific A11105-01) for 5min at 37°C. Cells were spun down at 1000RPM for 5min at RT. Cells were resuspended and plated in iN media (Neurobasal-A media (Invitrogen A24775-01) with 5mM glucose (Sigma G5146), 10mM sodium pyruvate (Sigma P5280), glutamax (Life Technologies 35050-061), penicillin/streptomycin (Thermo Fisher Scientific 15140-148), BDNF and NT-3 (10ng/mL), and doxycycline (2ug/mL) through 9 days. 2µM Ara-C (Sigma C6645) was added on DIV3, and there was a full media exchange 24 hours later (DIV4). Doxycycline post DIV10 was discontinued for the rest of the 21-day differentiation.

30

580

iAstrocyte differentiation of iPSCs

581

582 iPSCs transfected with the NGN2 virus were put through the first two days of the iNeuron

583 differentiation. On day 3, cells were exposed to Astrocyte differentiation media: N2 media

584 (without BDNF, NT-3, laminin, and doxycycline), 10% FBS (Hyclone SH30071.03HI), B-27 with

585 vitamin-A (Thermo Fisher Scientific 17504044), FGF-2 (20ng/mL, R&D Systems 233-FB-025) and

586 EGF (20ng/mL, R&D Systems 236-EG-200). After 30 days, EGF was removed and FGF2 reduced to

587 5ng/mL. After 70 total days, cells were switched into Astrocyte Media (Sciencell 1801).

588 Experiments were performed after 90 total days of differentiation. After DIV90, iAstrocyte stocks

589 were frozen down.

590

591 **iMicroglia differentiation of iPSCs**

592 iPSCs were differentiated into common myeloid progenitors (CMPs) according to the published

593 protocol (Paluru et al., 2014) by the Human Pluripotent Stem Cell Core (CHOP). CMPs were plated

594 at 333K cells / well in a 24-well Cellbind plate (Corning 3337). CMPs were differentiated in iMg

595 media (RPMI 1640 media (GE Healthcare Life Sciences SH30027.01) with 10% FBS (Hyclone

596 SH30071.03HI), Recombinant Human IL-34 (100ng/mL, R&D systems 5265-IL-010), CSF-1

597 Recombinant Human Protein (25ng/mL, Thermo Fisher Scientific PHC9504), and Recombinant

598 Human TGF-β1 (50ng/mL, Peprotech 100-21). Half media changes were performed every two

599 days for 11 days.

600

601 **Tri-culture combination**

602 iNeurons were differentiated as described above and re-plated on DIV2 to Matrigel (Corning

603 354230) coated Nunc Lab-Tek II 8-well chamber slides (Thermo Fisher Scientific 62407-296) at

604 70k cells/well in iN media. On DIV5 of iNeuron differentiation, the iAstrocytes were added at 50k

605 cells/well. On DIV7 of iNeuron differentiation, iMicroglia were added at 100k cell/well. Cultures

606 were taken out to DIV21 of iNeuron differentiation. Of note, this preparation creates a "carpet-

607 culture" of the three cell types that is roughly 50um thick

608

609 **Human astrocytes**

610 Three separate donors for human astrocytes were obtained from Sciencell. Cells were plated on

611 PLL-coated plates (Sigma Aldrich P6282) and grown for two weeks in Astrocyte media (Sciencell

612 1801) and then RNA was extracted.

613

614 **iAstrocyte cytokine exposure**

615 iAstrocytes in mono-culture were exposed to IL-1b (R&D Systems 201-LB-005) or IL-8 (R&D

616 Systems 208-IL-010) at 10ng/mL or PBS vehicle control for 8 hours. Supernatants were collected

617 and sent for cytokine analysis.

618

619 **HIV infection**

620 iMicroglia were differentiated to D11. On D11, they were exposed to 50ng/mL of JAGO strain HIV

621 (UPenn Center of Aids Research; CFAR) for 24 hours. Media was fully exchange after 24 hours

622 and collected. Full media exchanges occur every 3 days for 15 days. If antiretroviral treatment

623 was used, it was started on day 6 of infection and added with each media exchange. Efavirenz

624 (U.S. Pharmacopeia 1234103) was used at 20nM and Darunavir (Prezista TMC114) at 4.5μM.

625

626 **Monocyte-derived macrophage differentiation**

627 We receive donated buffy coat from New York Blood Center from three donors (D471, D446,

628 D470). Buffy coat was diluted 1:1 with PBS (without Ca^{2+} and Mg^{2+}) (Invitrogen 14190144). 15

629 mLs of Ficoll (Sigma Aldrich 26878-85-8) was added to 50mL conical tubes. 25mLs of Buffy

630 Coat/PBS was slowly layered onto the Ficoll. Samples were spun at 1200 rpm for 45 minutes with

631 no brake. The peripheral blood mononuclear cell (PBMC) layer was removed and placed into a

632 new 50mL conical tube, and the volume was brought up to 50mL with PBS. The PBMCs are spun

633 at 450Xg for 10 minutes. The supernatant was discarded, and the pellet resuspended in 10mLs

634 of Red Blood Cell Lysis buffer (Sigma Aldrich 11814389001). Cells were shaking at RT for 10

635 minutes. Volume was brought up to 50mLs in PBS and spun at 450Xg for 10minutes. The

636 supernatant was discarded, and the pellet was resuspended in DMEM with 10% FBS + Gentamicin

637 (Thermo Fisher Scientific 15750060). The PBMCs were plated on 6-well tissue culture plate for 5

32

638   days. On day 5, a full media exchange was performed and added 10ng/mL Human GM-CSF (Gold

639   Biotechnology 1120-03-20). A half media exchange was performed on day 7. At day 10, RNA was

640   collected from macrophages.

641

642   **RNA extraction**

643   Cells were washed twice with RT PBS, then lifted with StemPro accutase (Thermo Fisher Scientific

644   A11105-01) and spun down at 1,500 rpm for 5 min. Fresh cells were processed through

645   Qiashredder (Qiagen 79654) and RNeasy mini kit (Qiagen 74104) and frozen at -80ºC.

646

647   **Immunofluorescence**

648   Cells were washed twice with PBS, then fixed in 4% PFA (VWR TCP0018) for 15 min at RT. Cells

649   were washed 3x in PBS for 5 min at RT before being stored in PBS at 4°C. Cells are blocked in 5%

650   BSA (Sigma A9418) and 0.1% Triton X-100 (sigma X100) for 1 hr at RT. Sections use 0.3% Triton-X

651   100 in blocking buffer. Primary and secondary antibodies were diluted in blocking buffer. Cells

652   were incubated in primary antibodies overnight at 4°C. Cells were washed 3x 5min each at RT in

653   PBS-T (0.1% Tween20 (Sigma P9416). Secondary was performed at RT in the dark for 1 hour. Cells

654   were washed 3x 5min each at RT in PBS-T, then mounted with Prolong gold antifade (Life

655   Technologies P36930).

656   Antibodies used for immunofluorescence: Chicken anti-MAP2 (Abcam ab5392,

657   RRID:AB_2138153, 1:500); Mouse anti-PSD-95 clone K28/43 (NeuroMab 75-028,

658   RRID:AB_2292909, 1:500); Mouse anti-Synaptophysin clone SY38 (Millipore MAB5258-20UG,

659   RRID:AB_95185, 1:250); Mouse anti-Nestin clone 10C2 (Millipore MAB5326, RRID:AB_11211837,

660   1:200); Rabbit anti-Thrombospondin-1 (Abcam ab85762, RRID:AB_10674322, 1:250); Mouse

661   anti-Glutamine Synthetase (Millipore MAB302, RRID:AB_2110656, 1:500); Rabbit anti-SOX9

662   (Abcam ab185230, RRID:AB_2715497, 1:250); Rabbit anti-CX3CR1 (Abcam ab8021,

663   RRID:AB_306203, 1:500); Rabbit anti-TMEM119 (Abcam ab185333, RRID:AB_2687894, 1:200);

664   Rabbit anti-IBA1 (Wako 019-19741, RRID:AB_839504, 1:500); Rabbit anti-P2RY12 (Alomone Labs

665   APR-020, RRID:AB_11121048, 1:100); Rat anti-LAMP1 (Abcam ab25245, RRID:AB_449893,

666   1:500); Mouse anti- HIV1 p24 [39/5.4A] (Abcam ab9071, RRID:AB_306981, 1:500); Rabbit anti-

667 Human Nanog (Cell Signaling Technology 3580, RRID:AB_2150399, 1:800); Mouse anti-NCAM

668 Clone 2-2b (Millipore MAB5324, RRID:AB_95211, 1:250); Rabbit anti-OCT-4 (Cell Signaling

669 Technology 2750, RRID:AB_823583, 1:200); Rabbit anti-SOX2 (Millipore AB5603,

670 RRID:AB_2286686, 1:100); Rabbit anti-CCR5 (Thermo Fisher Scientific pa5-29011,

671 RRID:AB_2546487, 1:500); Mouse anti-GLAST (Miltenyi Biotec 130-095-822, RRID:AB_10829302,

672 1:50); Mouse anti-GFAP (Sigma-Aldrich SAB1405864, RRID:AB_10739114, 1:10,000); Mouse anti-

673 Beta-Actin (Cell Signaling Technology 3700, RRID:AB_2242334, 1:10,000); Rabbit anti-EAAC1

674 (Santa Cruz Biotechnology sc-25658, RRID:AB_2190727, 1:50); Rabbit GLT-1 (Jeff Rothstein Lab

675 1:5,000); Goat anti-mouse IgG (H+L) Alexa Fluor 488 (Thermo Fisher Scientific A-11029,

676 RRID:AB_138404, 1:500); Goat anti-rabbit IgG (H+L) Alexa Fluor 488 (Thermo Fisher Scientific A-

677 11034, RRID:AB_2576217, 1:500); Goat anti-mouse IgG (H+L) Alexa Fluor 568 (Thermo Fisher

678 Scientific A-11004, RRID:AB_2534072, 1:500); Goat anti-rabbit IgG (H+L) Alexa Fluor 568 (Thermo

679 Fisher Scientific A-11036, RRID:AB_10563566, 1:500); Goat anti-rat IgG (H+L) Alexa Fluor 568

680 (Molecular Probes A-11077, RRID:AB_141874, 1:500); Goat anti-rat IgG (H+L) Alexa Fluor 680

681 (Molecular Probes A-21096, RRID:AB_141554, 1:500); Goat anti-Chicken IgY (H+L) DyLight 680

682 (Thermo Fisher Scientific SA5-10074, RRID:AB_2556654, 1:500)

683

iAstrocyte immunofluorescence counting

685 Images were obtained with a Nikon eclipse N1 scope equipped with LED-based epifluorescence.

686 The optical fractionator workflow mode of Stereo Investigator 64 bit was then used to generate

687 random areas of the wells to image. 5 images were obtained per well. Images were then

688 transferred to image J where the channels were manually merged. After merging images, the

689 "cell count" plug in of imageJ is used to quantify the total number of DAPI (+) cells, and the

690 number of co-labeled DAPI+ astrocyte marker(+) cells.

691

Local Synapse Density

693 Images were analyzed on ImageJ. The iMicroglia were outlined and had a 50μm radius circle

694 drawn from the center of the cell with ROI manager. The total synapse density was measured

695 using the analyze particles plugin. The plugin was used for the ROI of the cell and the surrounding

696   circle. The area of the cell and the area of the particles were subtracted from the total area of

697   the circle and the total particles. The remaining total area of the particles was divided by the

698   remaining total area of the circle to calculate local synapse density.

699

700   **Bulk RNA-seq**

701   RNA was extracted using previously described with RNeasy mini kit (Qiagen 74104) and frozen at

702   -80°C. Samples were sent to the Center for Applied Genomics (CAG) for sequencing. In short, the

703   Illumina TruSeq Stranded Total RNA library kit (Illumina RS-122-2201) for RNA-seq was utilized

704   for preparation of the libraries for sequencing. Libraries were produced using liquid handler

705   automation with the PerkinElmer Sciclone instrument. This procedure started with a ribosomal

706   RNA (rRNA) depletion step. The depletion step uses target-specific oligos with specialized rRNA

707   removal beads to remove both cytoplasmic and mitochondrial rRNA from the total

708   RNA. Following this purification, the RNA was fragmented using a brief, high-temperature

709   incubation. The fragmented RNA was then reverse transcribed into first-strand cDNA using

710   reverse transcriptase and random primers. Second strand cDNA was generated using DNA

711   Polymerase which was then used in a standard TruSeq Illumina-adapter based library

712   preparation. Library preparation consisted of four main steps: unique adapter-indexes were

713   ligated to the RNA fragments, AmpureXP bead purification occurred to remove small library

714   fragments, the libraries were enriched and amplified using PCR, and the libraries underwent a

715   final purification using AmpureXP beads. Upon completion, library quality was assessed using an

716   automated electrophoresis instrument, the PerkinElmer Labchip GX Touch, and qPCR using the

717   Kapa Library Quantification Kit and Viia7 real-time PCR instrument. Libraries were diluted to the

718   appropriate sequencer loading concentration and pooled accordingly to allow for the desired

719   sequencing depth. RNA libraries were sequenced in one lane of the Illumina HiSeq2500

720   sequencer using the High Output v4 chemistry and paired-end sequencing (2x100bp).

721

722   **Single Cell RNA-seq cell preparation**

723   Cells were incubated in 0.25% Trypsin+EDTA at 37°C for 8 minutes, put through a cell strainer,

724   and spun down in ice-cold PBS at 4°C for 5 min at 1500 RPM. Cells were resuspended in ice-cold

725 DPBS without Mg^{2+} and Ca^{2+}+0.04% BSA. Up to 20,000 cells were sent for sequencing per sample.

726 Samples were sent to CAG for sequencing.

727

728 **Bulk RNA-seq analysis**

729 RNA-seq reads were demultiplexed using the DRAGEN genome pipeline (Goyal et al., 2017).

730 FASTQ files were aligned to hg19 reference using the STAR (v.2.6.1) (Dobin et al., 2013) aligner

731 with default settings. Generated BAM files were read into the R statistical computing

732 environment. Gene counts were obtained using the GenomicAlignments package. Differential

733 expression analysis was performed using the R/Bioconductor package DESeq2 which uses a

734 negative binomial model (Love, Huber, & Anders, 2014). Analysis was performed using standard

735 parameters with the independent filtering function enabled to filter genes with low mean

736 normalized counts. The Benjamini-Hochberg adjustment was used to estimate the false discovery

737 rate (Padj) and correct for multiple testing. Genes were then analyzed using the Ingenuity IPA

738 software (QIAGEN Inc.). Additional published RNA-seq data was utilized for comparative analysis

739 from project accession SRP092075 (Abud et al., 2017). Datasets were obtained and converted to

740 fastq format using the Sequence Read Archive (SRA) tool provided by NCBI. Fastq-formatted data

741 was analyzed similarly to the bulk RNA-seq samples using the DRAGEN pipeline and integrated

742 into the experimental R data object.

743

744 **Single Cell RNA-seq analysis**

745 Next-generation sequencing libraries were prepared using the 10x Genomics Chromium Single

746 Cell 3' Reagent kit v2 per manufacturer's instructions. Libraries were uniquely indexed using the

747 Chromium i7 Sample Index Kit, pooled, and sequenced on an Illumina Hiseq sequencer in a

748 paired-end, single indexing run. Sequencing for each library targeted 20,000 mean reads per cell.

749 We had a mean of 39,227 reads per cell post-normalization with 2,165 median genes per cell.

750 Data was then processed using the Cellranger pipeline (10x genomics, v.3.0.2) for demultiplexing

751 and alignment of sequencing reads to the GRCh38 transcriptome and creation of feature-barcode

752 matrices. Individual single cell RNAseq libraries were aggregated using the cellranger aggr

753 pipeline. Libraries were normalized for sequencing depth across all libraries during aggregation.

754 Secondary analysis on the aggregated feature barcode matrix was performed using the Seurat

755 package (v.3.0) within the R computing environment. Briefly, cells expressing less than 200 or

756 more than 5000 genes were excluded from further analysis. Additionally, cells expressing >20%

757 mitochondrial genes were excluded from the dataset. Log normalization and scaling of features

758 in the dataset was performed prior to principal component dimensionality reduction, clustering,

759 and visualization using tSNE. Cell types were identified using expression of canonical cell markers

760 in microglia (AIF1, SPI1, CD4), neurons (MAP2, SYN1), and astrocytes (THBS1, SOX9). Differentially

761 expressed genes and identification of cluster or cell type specific markers were identified using a

762 wilcoxon rank sum test between two groups. P-value adjustment was performed using

763 bonferroni correction based on total number of genes in the aggregated dataset. Genes were

764 then analyzed using the Ingenuity IPA software (QIAGEN Inc.).

765

766 **qRT-PCR**

767 RNA was extracted by RNeasy mini kit (Qiagen 74104). cDNA was generated using SuperScript

768 VILO Master mix (Thermo Fisher Scientific 11755050). RNA expression was measured using

769 Taqman probes (Thermo Fisher Scientific) for *CX3CR1* (Hs01922583_s1), *P2RY12*

770 (Hs01881698_s1), *TMEM119* (Hs01938722_u1), *THBS1* (Hs00962908_m1), and *GAPDH*

771 (Hs02786624_g1). 30ng of cDNA was used per well, with three technical replicates per probe per

772 sample. qRT-PCR is run on an Applied Biosystems 7900HT Fast Real-Time PCR System. All

773 expression levels were normalized to *GAPDH* expression.

774

775 **Reverse transcriptase activity**

776 10 µl per well of supernatant was placed into a 96-well microtiter plate to be analyzed for RT

777 activity. 50 µl of RT cocktail was added per well into the 96-well microtiter plate. RT cocktail

778 consists of: 50mM Tris (Amresco J837) pH 7.8, 75mM KCl (Ambion 9610), 2mM Dithiothreitol

779 (DTT) (Sigma D0632), 5mM Magnesium Chloride (Ambion 9530G), 5ug/mL Polyadenylic acid (GE

780 Healthcare 27-4110-01), 2.5ug/mL pd (t)12-18 (Oligo dT) (USB Corporation #19817), 0.05% NP-

781 40 (Calbiochem, 492016), 10 µCi/ml Thymidine 5'-triphosphate, ALPHA-[32P] / [32P] TTP (Perkin

782 Elmer BLU005A250MC). Samples were incubated at 37° C overnight. 30 µl of RT reaction mixture

783   was placed onto pre-marked DE81 paper (Whatman 3658915) and air dried for 15 min at RT.

784   Paper was washed 4x, 5 min each with 2x SSC (Roche-Apply science 11 666 681 001) by

785   submerging in a tray on a rotating platform. Paper was then washed 1x, 1 min in 100% ethanol

786   and air dried in an oven at 80-100° C (25-30 min). Each paper sample was placed into a

787   scintillation vial. 5 ml Betaflour (National Diagnostics LS-151) was added to each scintillation vial.

788   32P was counted on a scintillation counter, yielding CPM.

789

790   **PCR for CCR5Δ32 mutation**

791   DNA was isolated with DNeasy blood and tissue kit (Qiagen 69504). DNA Oligos were generated

792   by IDT. Forward primer: 5' – CAAAAAGAAGGTCTTCATTACACC – 3'. Reverse primer: 5' –

793   CCTGTGCCTCTTCTTCTCATTTCG – 3'. Primers were reconstituted to 100uM. Mastermix consists

794   of 10uL KAPA PCR buffer, 7uL H20, 1uL 10uM forward primer, 1uL 10uM reverse primer. 1uL DNA

795   added separately. 1.5% agarose gel was run for 1hour at 120v. The gel was imaged on a Biorad

796   Universal Hood II Gel Doc System.

797

798   **Western Blot**

799   iAst plated in 12-well dishes were rinsed twice with PBS containing 0.1 mM Ca^{2+} and 1.0 mM

800   Mg^{2+} (PBS Ca^{2+}/Mg^{2+}) then lysed in 200ul of radioimmunoprecipitation (RIPA) buffer (100 mM

801   Tris-HCl, pH 7.4, 150 mM NaCl, 1 mM EDTA, 0.1% SDS, 1% Triton X-100, 1% sodium deoxycholate

802   containing protease inhibitors, including 1 mg/ml leupeptin, 250 mM phenylmethylsulfonyl

803   fluoride, 1 mg/ml aprotinin, and 1 mM iodoacetamide) for 1 hour while rotating on a shaker at

804   4°C. Cortical and hippocampal tissue was harvested from adult C57BL/6 mice and solubilized in

805   5 volumes of homogenization buffer (50 mM Tris-HCl, pH 7.4, 150 mM NaCl, 5 mM EDTA, 1% NP-

806   40, 1% SDS, containing protease and phosphatase inhibitors, including 1 mg/ml leupeptin,

807   250 mM phenylmethylsulfonyl fluoride, 1 mg/ml aprotinin, 1 mM iodoacetamide, 10mM NaF,

808   30mM Na pyrophosphate, 1mM Na^3VO^4). All lysates were centrifuged at 17,000g for 20 min to

809   remove cellular debris and nuclei. The supernatants were analyzed for total protein using the

810   Pierce protein assay kit according to the manufacturer's instructions. Lysates are diluted 1:1 with

811   2X Laemmli buffer and either boiled at 95°C for 5 min (GFAP, Actin) or kept at 25°C for 45 minutes

812   (GLAST, GLT-1, EAAC1). iAst lysates (20ug) or cortical/hippocampal lysates (5ug) were then

813   resolved by SDS PAGE using 10% BioRad minigels and transferred to Immobilon-FL membranes

814   (Millipore Cat# IPFL00010). Membranes were incubated with blocking buffer (1% non-fat dry

815   milk in TBS-T) for 1 hour at 25°C prior to probing with primary antibodies diluted in blocking

816   buffer overnight at 4°C: rabbit anti-GLT-1 (C-terminal directed 1:5,000; Rothstein et al 1994),

817   mouse anti-GLAST (Miltenyi Biotec Cat# 130-095-822, 1:50), rabbit anti-EAAC1 (Santa Cruz Cat#

818   SC-25658, 1:50), mouse anti-GFAP (Cell Signaling Cat#3670S, 1:1,000), and mouse anti-Actin

819   (1:10,000 dilution, Cell Signaling, Cat# 3700S). Membranes were washed with blocking buffer 3

820   times for 10 min at 25°C. After the washes, membranes were probed with anti-mouse or anti-

821   rabbit fluorescently conjugated secondary antibodies (LI-COR Biosystems, 1:10,000) for 45

822   minutes at 25°C. The membranes were washed 3 times for 10 minutes each then visualized using

823   a LI-COR Odyssey.

824

825   **Synaptophagocytosis analysis**

826   Confocal images of microglia were analyzed in IMARIS software. IBA1 labeling for the microglia

827   was surfaced, as well as synaptophysin staining. Total volume was taken for the microglia and

828   the synaptophysin staining inside the cells. Total synaptophysin volume per cell was then divided

829   by the cell volume defined by IBA1 labeling.

830

831   **Cytokine analysis**

832   Supernatants were tested for 6 analytes (TNFa, IL-6, IL-8, IL-10, IL-1b, IL-1a) on a custom Human

833   magnetic Luminex plate (R&D systems LXSAHM; run by Penn Mental Health AIDS Research Center

834   (PMHARC)). The plate was run by the Penn Mental Health Aids Research Center on a MAGPIX

835   powered by Luminex XMAP technology.

References

Abud, E. M., Ramirez, R. N., Martinez, E. S., Healy, L. M., Nguyen, C. H. H. H. H., Newman, S. A., . . . Blurton-Jones, M. (2017). iPSC-Derived Human Microglia-like Cells to Study Neurological Diseases. *Neuron, 94*(2), 278-293.e279-293.e279. doi:10.1016/j.neuron.2017.03.042

Akay, C., Cooper, M., Odeleye, A., Jensen, B. K., White, M. G., Vassoler, F., . . . Jordan-Sciutto, K. L. (2014). Antiretroviral drugs induce oxidative stress and neuronal damage in the central nervous system. *Journal of NeuroVirology, 20*(1), 39-53-53. doi:10.1007/s13365-013-0227-1

Akay, C., Lindl, K. A., Shyam, N., Nabet, B., Goenaga-Vazquez, Y., Ruzbarsky, J., . . . Jordan-Sciutto, K. L. (2012). Activation status of integrated stress response pathways in neurones and astrocytes of HIV-associated neurocognitive disorders (HAND) cortex. *Neuropathol Appl Neurobiol, 38*(2), 175-200. doi:10.1111/j.1365-2990.2011.01215.x

Awabdh, S. A., Gupta-Agarwal, S., Sheehan, D. F., Muir, J., Norkett, R., Twelvetrees, A. E., . . . Kittler, J. T. (2016). Neuronal activity mediated regulation of glutamate transporter GLT-1 surface diffusion in rat astrocytes in dissociated and slice cultures. *Glia, 64*(7), 1252-1264-1264. doi:10.1002/glia.22997

Best, B. M., & Goicoechea, M. (2008). Efavirenz – Still First-line King? *Expert Opinion on Drug Metabolism & Toxicology, 4*(7), 965-972-972. doi:10.1517/17425255.4.7.965

Carey, A. N., Sypek, E. I., Singh, H. D., Kaufman, M. J., & McLaughlin, J. P. (2012). Expression of HIV-Tat protein is associated with learning and memory deficits in the mouse. *Behavioural Brain Research, 229*(1), 48-56-56. doi:10.1016/j.bbr.2011.12.019

Chen, W., Sulcove, J., Frank, I., Jaffer, S., Ozdener, H., & Kolson, D. L. (2002). Development of a human neuronal cell model for human immunodeficiency virus (HIV)-infected macrophage-induced neurotoxicity: apoptosis induced by HIV type 1 primary isolates and evidence for involvement of the Bcl-2/Bcl-xL-sensitive intrinsic apoptosis pathway. *Journal of Virology, 76*(18), 9407-9419-9419. doi:10.1128/JVI.76.18.9407-9419.2002

Cho, S. H., Chen, J. A., Sayed, F., Ward, M. E., Gao, F., Nguyen, T. A., . . . Gan, L. (2015). SIRT1 deficiency in microglia contributes to cognitive decline in aging and neurodegeneration via epigenetic regulation of IL-1beta. *J Neurosci, 35*(2), 807-818. doi:10.1523/JNEUROSCI.2939-14.2015

Christopherson, K. S., Ullian, E. M., Stokes, C. C., Mullowney, C. E., Hell, J. W., Agah, A., . . . Barres, B. A. (2005). Thrombospondins are astrocyte-secreted proteins that promote CNS synaptogenesis. *Cell, 120*(3), 421-433. doi:10.1016/j.cell.2004.12.020

Ciccarelli, N., Fabbiani, M., Di Giambenedetto, S., Fanti, I., Baldonero, E., Bracciale, L., . . . Silveri, M. C. (2011). Efavirenz associated with cognitive disorders in otherwise asymptomatic HIV-infected patients. *Neurology, 76*(16), 1403. doi:10.1212/WNL.0b013e31821670fb

Clark, J., Vagenas, P., Panesar, M., & Cope, A. P. (2005). What does tumour necrosis factor excess do to the immune system long term? *Annals of the Rheumatic Diseases, 64*(suppl 4), iv70. doi:10.1136/ard.2005.042523

Cui, W., Li, J., Ron, D., & Sha, B. (2011). The structure of the PERK kinase domain suggests the mechanism for its activation. *Acta Crystallographica Section D: Biological Crystallography, 67*(5), 423-428-428. doi:10.1107/S0907444911006445

889 Cummins, N. W., & Badley, A. D. (2010). Mechanisms of HIV-associated lymphocyte apoptosis:
890   2010. *Cell Death & Disease, 1*(11), e99. doi:10.1038/cddis.2010.77

891 D'Aversa, T. G., Eugenin, E. A., & Berman, J. W. (2008). CD40-CD40 ligand interactions in human
892   microglia induce CXCL8 (interleukin-8) secretion by a mechanism dependent on activation
893   of ERK1/2 and nuclear translocation of nuclear factor-kappaB (NFkappaB) and activator
894   protein-1 (AP-1). *J Neurosci Res, 86*(3), 630-639. doi:10.1002/jnr.21525

895 De Clercq, E. (2004). Non-Nucleoside Reverse Transcriptase Inhibitors (NNRTIs): Past, Present,
896   and Future. *Chemistry & Biodiversity, 1*(1), 44-64-64. doi:10.1002/cbdv.200490012

897 Debaisieux, S., Lachambre, S., Gross, A., Mettling, C., Besteiro, S., Yezid, H., . . . Beaumelle, B.
898   (2015). HIV-1 Tat inhibits phagocytosis by preventing the recruitment of Cdc42 to the
899   phagocytic cup. *Nat Commun, 6*, 6211. doi:10.1038/ncomms7211

900 Deng, H., Liu, R., Ellmeier, W., Choe, S., Unutmaz, D., Burkhart, M., . . . Landau, N. R. (1996).
901   Identification of a major co-receptor for primary isolates of HIV-1. *Nature, 381*(6584),
902   661-666-666. doi:10.1038/381661a0

903 Dirk, B. S., Pawlak, E. N., Johnson, A. L., Nynatten, L. R., Jacob, R. A., Heit, B., & Dikeakos, J. D.
904   (2016). HIV-1 Nef sequesters MHC-I intracellularly by targeting early stages of endocytosis
905   and recycling. *Scientific Reports, 6*, 37021. doi:10.1038/srep37021

906 Dobin, A., Davis, C. A., Schlesinger, F., Drenkow, J., Zaleski, C., Jha, S., . . . Gingeras, T. R. (2013).
907   STAR: ultrafast universal RNA-seq aligner. *Bioinformatics, 29*(1), 15-21-21.
908   doi:10.1093/bioinformatics/bts635

909 Fuster, J. M., Bodner, M., & Kroger, J. K. (2000). Cross-modal and cross-temporal association in
910   neurons of frontal cortex. *Nature, 405*(6784), 347. doi:10.1038/35012613

911 Ginsberg, S. D., Alldred, M. J., Gunnam, S. M., Schiroli, C., Lee, S. H., Morgello, S., & Fischer, T.
912   (2018). Expression profiling suggests microglial impairment in human immunodeficiency
913   virus neuropathogenesis. *Ann Neurol, 83*(2), 406-417. doi:10.1002/ana.25160

914 Giunta, B., Ehrhart, J., Obregon, D. F., Lam, L., Le, L., Jin, J., . . . Shytle, R. D. (2011). Antiretroviral
915   medications disrupt microglial phagocytosis of β-amyloid and increase its production by
916   neurons: implications for HIV-associated neurocognitive disorders. *Mol Brain, 4*(1), 23.
917   doi:10.1186/1756-6606-4-23

918 Giunta, B., Zhou, Y., Hou, H., Rrapo, E., Fernandez, F., & Tan, J. (2008). HIV-1 TAT inhibits
919   microglial phagocytosis of Abeta peptide. *Int J Clin Exp Pathol, 1*(3), 260-275.

920 Goyal, A., Kwon, H. J., Lee, K., Garg, R., Yun, S. Y., Kim, Y. H., . . . Lee, M. S. (2017). Ultra-Fast Next
921   Generation Human Genome Sequencing Data Processing Using DRAGEN^{TM}
922   Bio-IT Processor for Precision Medicine. *Open Journal of Genetics, 07*(01), 9-19-19.
923   doi:10.4236/ojgen.2017.71002

924 Haenseler, W., Sansom, S. N., Buchrieser, J., Newey, S. E., Moore, C. S., Nicholls, F. J., . . . Cowley,
925   S. A. (2017). A Highly Efficient Human Pluripotent Stem Cell Microglia Model Displays a
926   Neuronal-Co-culture-Specific Expression Profile and Inflammatory Response. *Stem Cell
927   Reports, 8*(6), 1727-1742. doi:10.1016/j.stemcr.2017.05.017

928 Homig-Holzel, C., Hojer, C., Rastelli, J., Casola, S., Strobl, L. J., Muller, W., . . . Zimber-Strobl, U.
929   (2008). Constitutive CD40 signaling in B cells selectively activates the noncanonical NF-
930   kappaB pathway and promotes lymphomagenesis. *J Exp Med, 205*(6), 1317-1329.
931   doi:10.1084/jem.20080238

932   Hong, S., Beja-Glasser, V. F., Nfonoyim, B. M., Frouin, A., Li, S., Ramakrishnan, S., . . . Stevens, B.
933   (2016). Complement and microglia mediate early synapse loss in Alzheimer mouse
934   models. *Science*, aad8373. doi:10.1126/science.aad8373
935   Janssens, S., Pulendran, B., & Lambrecht, B. N. (2014). Emerging functions of the unfolded protein
936   response in immunity. *Nature Immunology, 15*(10), 910-919-919. doi:10.1038/ni.2991
937   Jesko, H., Wencel, P., Strosznajder, R. P., & Strosznajder, J. B. (2017). Sirtuins and Their Roles in
938   Brain Aging and Neurodegenerative Disorders. *Neurochem Res, 42*(3), 876-890.
939   doi:10.1007/s11064-016-2110-y
940   Kang, P., Lee, Hyun K., Glasgow, Stacey M., Finley, M., Donti, T., Gaber, Zachary B., . . . Deneen,
941   B. (2012). Sox9 and NFIA Coordinate a Transcriptional Regulatory Cascade during the
942   Initiation of Gliogenesis. *Neuron, 74*(1), 79-94-94. doi:10.1016/j.neuron.2012.01.024
943   Keren-Shaul, H., Spinrad, A., Weiner, A., Matcovitch-Natan, O., Dvir-Szternfeld, R., Ulland, T. K., .
944   . . Amit, I. (2017). A Unique Microglia Type Associated with Restricting Development of
945   Alzheimer's Disease. *Cell, 169*(7), 1276-1290 e1217. doi:10.1016/j.cell.2017.05.018
946   Kim, B. O., Liu, Y., Ruan, Y., Xu, Z. C., Schantz, L., & He, J. J. (2003). Neuropathologies in Transgenic
947   Mice Expressing Human Immunodeficiency Virus Type 1 Tat Protein under the Regulation
948   of the Astrocyte-Specific Glial Fibrillary Acidic Protein Promoter and Doxycycline. *The
949   American Journal of Pathology, 162*(5), 1693-1707-1707. doi:10.1016/s0002-
950   9440(10)64304-0
951   Kim, Y.-S., Morgan, M. J., Choksi, S., & Liu, Z.-g. (2007). TNF-Induced Activation of the Nox1
952   NADPH Oxidase and Its Role in the Induction of Necrotic Cell Death. *Molecular Cell, 26*(5),
953   675-687-687. doi:10.1016/j.molcel.2007.04.021
954   Kolson, D. (2017). Neurologic Complications in Persons With HIV Infection in the Era of
955   Antiretroviral Therapy. *Topics in antiviral medicine, 25*(3), 97-101-101. Retrieved from
956   http://www.ncbi.nlm.nih.gov/pubmed/28820724
957   Kornbluth, R. S. (2000). The emerging role of CD40 ligand in HIV infection. *Journal of Leukocyte
958   Biology, 68*(3), 373-382. doi:10.1189/jlb.68.3.373
959   Langford, D., Kim, B. o., Zou, W., Fan, Y., Rahimain, P., Liu, Y., & He, J. J. (2018). Doxycycline-
960   inducible and astrocyte-specific HIV-1 Tat transgenic mice (iTat) as an HIV/neuroAIDS
961   model. *Journal of NeuroVirology, 24*(2), 168-179-179. doi:10.1007/s13365-017-0598-9
962   Lendahl, U., Zimmerman, L. B., & McKay, R. D. G. (1990). CNS stem cells express a new class of
963   intermediate filament protein. *Cell, 60*(4), 585-595-595. doi:10.1016/0092-
964   8674(90)90662-x
965   Liddelow, S. A., Guttenplan, K. A., Clarke, L. E., Bennett, F. C., Bohlen, C. J., Schirmer, L., . . . Barres,
966   B. A. (2017). Neurotoxic reactive astrocytes are induced by activated microglia. *Nature,
967   541*(7638), 481-487-487. doi:10.1038/nature21029
968   Lin, Y.-T., Seo, J., Gao, F., Feldman, H. M., Wen, H.-L., Penney, J., . . . Tsai, L.-H. (2018). APOE4
969   Causes Widespread Molecular and Cellular Alterations Associated with Alzheimer's
970   Disease Phenotypes in Human iPSC-Derived Brain Cell Types. *Neuron, 98*(6), 1141-
971   1154.e1147-1154.e1147. doi:10.1016/j.neuron.2018.05.008
972   Lindl, K. A., Akay, C., Wang, Y., White, M. G., & Jordan-Sciutto, K. L. (2007). Expression of the
973   endoplasmic reticulum stress response marker, BiP, in the central nervous system of HIV-
974   positive individuals. *Neuropathol Appl Neurobiol, 33*(6), 658-669. doi:10.1111/j.1365-
975   2990.2007.00866.x

976   Lindl, K. A., Akay, C., Wang, Y., White, M. G., & Jordan-Sciutto, K. L. (2007). Expression of the
977   endoplasmic reticulum stress response marker, BiP, in the central nervous system of HIV-
978   positive individuals. *Neuropathology and Applied Neurobiology, 33*(6), 658-669-669.
979   doi:10.1111/j.1365-2990.2007.00866.x

980   Lindl, K. A., Marks, D. R., Kolson, D. L., & Jordan-Sciutto, K. L. (2010). HIV-Associated
981   Neurocognitive Disorder: Pathogenesis and Therapeutic Opportunities. *Journal of
982   Neuroimmune Pharmacology, 5*(3), 294-309-309. doi:10.1007/s11481-010-9205-z

983   Liu, R., Paxton, W. A., Choe, S., Ceradini, D., Martin, S. R., Horuk, R., . . . Landau, N. R. (1996).
984   Homozygous Defect in HIV-1 Coreceptor Accounts for Resistance of Some Multiply-
985   Exposed Individuals to HIV-1 Infection. *Cell, 86*(3), 367-377-377. doi:10.1016/s0092-
986   8674(00)80110-5

987   Love, M. I., Huber, W., & Anders, S. (2014). Moderated estimation of fold change and dispersion
988   for RNA-seq data with DESeq2. *Genome Biology, 15*(12), 550. doi:10.1186/s13059-014-
989   0550-8

990   Lui, H., Zhang, J., Makinson, S. R., Cahill, M. K., Kelley, K. W., Huang, H. Y., . . . Huang, E. J. (2016).
991   Progranulin Deficiency Promotes Circuit-Specific Synaptic Pruning by Microglia via
992   Complement Activation. *Cell, 165*(4), 921-935. doi:10.1016/j.cell.2016.04.001

993   Marmur, R., Mabie, P. C., Gokhan, S., Song, Q., Kessler, J. A., & Mehler, M. F. (1998). Isolation and
994   Developmental Characterization of Cerebral Cortical Multipotent Progenitors.
995   *Developmental Biology, 204*(2), 577-591-591. doi:10.1006/dbio.1998.9099

996   Masterman, D. L., & Cummings, J. L. (1997). Frontal-subcortical circuits: the anatomic basis of
997   executive, social and motivated behaviors. *Journal of Psychopharmacology, 11*(2), 107-
998   114-114. doi:10.1177/026988119701100203

999   Masuda, M., Miyazaki-Anzai, S., Levi, M., Ting, T. C., & Miyazaki, M. (2013). PERK-eIF2alpha-ATF4-
1000   CHOP signaling contributes to TNFalpha-induced vascular calcification. *J Am Heart Assoc,
1001   2*(5), e000238. doi:10.1161/JAHA.113.000238

1002   Mazzolini, J., Herit, F., Bouchet, J., Benmerah, A., Benichou, S., & Niedergang, F. (2010). Inhibition
1003   of phagocytosis in HIV-1-infected macrophages relies on Nef-dependent alteration of
1004   focal delivery of recycling compartments. *Blood, 115*(21), 4226-4236. doi:10.1182/blood-
1005   2009-12-259473

1006   Miller, E. K. (2000). The prefontral cortex and cognitive control. *Nature Reviews Neuroscience,
1007   1*(1), 35036228. doi:10.1038/35036228

1008   O'Donnell, L. A., Agrawal, A., Jordan-Sciutto, K. L., Dichter, M. A., Lynch, D. R., & Kolson, D. L.
1009   (2006). Human immunodeficiency virus (HIV)-induced neurotoxicity: roles for the NMDA
1010   receptor subtypes. *The Journal of neuroscience : the official journal of the Society for
1011   Neuroscience, 26*(3), 981-990-990. doi:10.1523/jneurosci.4617-05.2006

1012   Paluru, P., Hudock, K. M., Cheng, X., Mills, J. A., Ying, L., Galvão, A. M., . . . Gadue, P. (2014). The
1013   negative impact of Wnt signaling on megakaryocyte and primitive erythroid progenitors
1014   derived from human embryonic stem cells. *Stem Cell Research, 12*(2), 441-451-451.
1015   doi:10.1016/j.scr.2013.12.003

1016   Park, J., Wetzel, I., Marriott, I., Dréau, D., D'Avanzo, C., Kim, D. Y., . . . Cho, H. (2018). A 3D human
1017   triculture system modeling neurodegeneration and neuroinflammation in Alzheimer's
1018   disease. *Nature Neuroscience*, 1-13-13. doi:10.1038/s41593-018-0175-4

1019 Perego, C., Vanoni, C., Bossi, M., Massari, S., Basudev, H., Longhi, R., & Pietrini, G. (2000). The
1020   GLT-1 and GLAST Glutamate Transporters Are Expressed on Morphologically Distinct
1021   Astrocytes and Regulated by Neuronal Activity in Primary Hippocampal Cocultures.
1022   *Journal of Neurochemistry, 75*(3), 1076-1084-1084. doi:10.1046/j.1471-
1023   4159.2000.0751076.x
1024 Reid, W., Sadowska, M., Denaro, F., Rao, S., Foulke, J., Hayes, N., . . . Bryant, J. (2001). An HIV-1
1025   transgenic rat that develops HIV-related pathology and immunologic dysfunction.
1026   *Proceedings of the National Academy of Sciences, 98*(16), 9271-9276-9276.
1027   doi:10.1073/pnas.161290298
1028 Robertson, K., Liner, J., & Meeker, R. B. (2012). Antiretroviral neurotoxicity. *Journal of
1029   NeuroVirology, 18*(5), 388-399-399. doi:10.1007/s13365-012-0120-3
1030 Salter, M. W., & Stevens, B. (2017). Microglia emerge as central players in brain disease. *Nature
1031   Medicine, 23*(9), 1018-1027-1027. doi:10.1038/nm.4397
1032 Santos, R., Vadodaria, K. C., Jaeger, B. N., Mei, A., Lefcochilos-Fogelquist, S., Mendes, A. P. D., . .
1033   . Gage, F. H. (2017). Differentiation of Inflammation-Responsive Astrocytes from Glial
1034   Progenitors Generated from Human Induced Pluripotent Stem Cells. *Stem Cell Reports,
1035   8*(6), 1757-1769. doi:10.1016/j.stemcr.2017.05.011
1036 Saylor, D., Dickens, A. M., Sacktor, N., Haughey, N., Slusher, B., Pletnikov, M., . . . McArthur, J. C.
1037   (2016). HIV-associated neurocognitive disorder--pathogenesis and prospects for
1038   treatment. *Nature reviews. Neurology, 12*(4), 234-248-248.
1039   doi:10.1038/nrneurol.2016.27
1040 Spinner, C. D., Boesecke, C., Zink, A., Jessen, H., Stellbrink, H.-J., Rockstroh, J. K., & Esser, S. (2016).
1041   HIV pre-exposure prophylaxis (PrEP): a review of current knowledge of oral systemic HIV
1042   PrEP in humans. *Infection, 44*(2), 151-158-158. doi:10.1007/s15010-015-0850-2
1043 Stutzbach, L. D., Xie, S. X., Naj, A. C., Albin, R., Gilman, S., Lee, V. M. Y., . . . Group, P. S. P. (2013).
1044   The unfolded protein response is activated in disease-affected brain regions in
1045   progressive supranuclear palsy and Alzheimer's disease. *Acta Neuropathologica
1046   Communications, 1*(1), 1-13-13. doi:10.1186/2051-5960-1-31
1047 Sui, Z., Sniderhan, L. F., Schifitto, G., Phipps, R. P., Gelbard, H. A., Dewhurst, S., & Maggirwar, S.
1048   B. (2007). Functional synergy between CD40 ligand and HIV-1 Tat contributes to
1049   inflammation: implications in HIV type 1 dementia. *J Immunol, 178*(5), 3226-3236.
1050   doi:10.4049/jimmunol.178.5.3226
1051 Swanson, R. A., Liu, J., Miller, J. W., Rothstein, J. D., Farrell, K., Stein, B. A., & Longuemare, M. C.
1052   (1997). Neuronal Regulation of Glutamate Transporter Subtype Expression in Astrocytes.
1053   *Journal of Neuroscience, 17*(3), 932-940-940. doi:10.1523/jneurosci.17-03-00932.1997
1054 Taramasso, L., Biagio, A. D., Maggiolo, F., Tavelli, A., Caputo, S. L., Bonora, S., . . . Group, t. I. C. N.
1055   A. F. S. (2018). First-line antiretroviral therapy with efavirenz plus tenofovir disiproxil
1056   fumarate/emtricitabine or rilpivirine plus tenofovir disiproxil fumarate/emtricitabine: a
1057   durability comparison. *HIV Medicine, 19*(7), 475-484-484. doi:10.1111/hiv.12628
1058 Tatro, E. T., Soontornniyomkij, B., Letendre, S. L., & Achim, C. L. (2014). Cytokine secretion from
1059   brain macrophages infected with human immunodeficiency virus in vitro and treated with
1060   raltegravir. *BMC Infectious Diseases, 14*(1), 386. doi:10.1186/1471-2334-14-386
1061 Turchan–Cholewo, J., Dimayuga, V. M., Gupta, S., Gorospe, R. M. C., Keller, J. N., & Bruce–Keller,
1062   A. J. (2009). NADPH Oxidase Drives Cytokine and Neurotoxin Release from Microglia and

1063   Macrophages in Response to HIV-Tat. *Antioxidants & Redox Signaling, 11*(2), 193-204.
1064   doi:10.1089/ars.2008.2097

1065 Walter, P., & Ron, D. (2011). The Unfolded Protein Response: From Stress Pathway to
1066   Homeostatic Regulation. *Science, 334*(6059), 1081-1086-1086.
1067   doi:10.1126/science.1209038

1068 Wilkinson, B. L., & Landreth, G. E. (2006). The microglial NADPH oxidase complex as a source of
1069   oxidative stress in Alzheimer's disease. *J Neuroinflammation, 3*, 30. doi:10.1186/1742-
1070   2094-3-30

1071 Wood, A. J. J., & Flexner, C. (1998). HIV-Protease Inhibitors. *The New England Journal of Medicine,*
1072   *338*(18), 1281-1293-1293. doi:10.1056/nejm199804303381808

1073 Zhang, Y., Pak, C., Han, Y., Ahlenius, H., Zhang, Z., Chanda, S., . . . Südhof, T. C. (2013). Rapid Single-
1074   Step Induction of Functional Neurons from Human Pluripotent Stem Cells. *Neuron, 78*(5).
1075   doi:10.1016/j.neuron.2013.05.029

1076 Zrzavy, T., Hametner, S., Wimmer, I., Butovsky, O., Weiner, H. L., & Lassmann, H. (2017). Loss of
1077   'homeostatic' microglia and patterns of their activation in active multiple sclerosis. *Brain,*
1078   *140*(7), 1900-1913-1913. doi:10.1093/brain/awx113

1079

1080 The datasets generated during and/or analyzed during the current study are available in the GEO
1081 repository, [LinkOnceObtainedFromGEO]